USAFA TR 91-13

COMPARISON OF STATION-KEEPING ALGORITHMS FOR AN INTERIOR LIBRATION POINT ORBIT IN THE SUN-EARTH+MOON ELLIPTIC RESTRICTED THREE-BODY PROBLEM

STEVEN C. GORDON, LT COL, USAF
DEPARTMENT OF OF MATHEMATICAL SCIENCES

OCTOBER 1991
FINAL REPORT

DEAN OF THE FACULTY
UNITED STATES AIR FORCE ACADEMY
COLORADO 80840

USAFA-TR-91-13

Technical Review by Captain Rich Schooff
Department of Mathematical Science
USAFA Academy, Colorado 80840

Technical Review by Lt Col Daryl G. Boden
Department of Astronautics
USAF Academy, Colorado 80840

Editorial Review by Lt Col Donald C. Anderson
Department of English
USAF Academy, Colorado 80840

This research report entitled "Comparison of Station-Keeping Algorithms For An Interior Libration Point Orbit In The Sun-Earth+Moon Elliptic Restricted Three-Body Problem" is presented as a competent treatment of the subject, worthy of publication. The United States Air Force Academy vouches for the quality of the research, without necessarily endorsing the opinions and conclusions of the author.

This report has been cleared for open publication and public release by the appropriate Office of Information in accordance with AFM 190-1, AFR 12-30, and AFR 80-3. This report may have unlimited distribution.

Robert K. Morrow, Jr.

ROBERT K. MORROW JR., Lt Col, USAF
Director of Research

17 SEP 91
Dated

REPORT DOCUMENTATION PAGE

Form Approved
OMB No 0704 0188

1. AGENCY USE ONLY (Leave blank)	2. REPORT DATE	3. REPORT TYPE AND DATES COVERED
	10 Oct 1991	Final

4. TITLE AND SUBTITLE
Comparison of Station-Keeping Algorithms For An Interior Libration Point Orbit in the Sun-Earth+Moon Elliptic Restricted Three-Body Problem

5. FUNDING NUMBERS
PR 37731G

6. AUTHOR(S)
Steven C. Gordon, Lt Col, USAF

7. PERFORMING ORGANIZATION NAME(S) AND ADDRESS(ES)
Department of Mathematical Sciences
United States Air Force Academy, Colorado 80840

8. PERFORMING ORGANIZATION REPORT NUMBER
USAFATR 91-13

9. SPONSORING/MONITORING AGENCY NAME(S) AND ADDRESS(ES)
Frank J. Seiler Research Laboratory
United States Air Force Academy, Colorado 80840

10. SPONSORING/MONITORING AGENCY REPORT NUMBER

11. SUPPLEMENTARY NOTES
Research conducted under the direction of Prof K. C. Howell, School of Aeronautics and Astronautics, Purdue University

12a. DISTRIBUTION/AVAILABILITY STATEMENT

12b. DISTRIBUTION CODE

13. ABSTRACT (Maximum 200 words)

A spacecraft near a Lagrange (libration) point orbit between the Earth and the Sun can study the important interaction of the Sun's corona with the terrestrial environment. However, the spacecraft will drift from the nominal (unstable) path. The accumulated error in the spacecraft's position and velocity relative to the nominal path after a predetermined period of range and range-rate tracking can be computed. This error, or uncertainty, in the spacecraft state is measured through simulations, commonly referred to as orbit determination error analysis, and is presented as either variances or standard deviations of the state vector elements. The state uncertainty computed in the error analysis can then be input to a station-keeping algorithm. The algorithm computes control maneuvers that return the spacecraft to the vicinity of the nominal path. Variations in orbital shapes and sizes may, however, have some effect on the station-keeping costs. Several algorithms are derived and are used to test differences in station-keeping costs for orbits of different size and shape. Statistical hypothesis tests for equality of means are used in the comparisons.

14. SUBJECT TERMS	15. NUMBER OF PAGES
Libration points, three-body problem, least squares, spacecraft orbits, station-keeping, optimal control, state feedback control, hypothesis tests	102
	16. PRICE CODE

17. SECURITY CLASSIFICATION OF REPORT	18. SECURITY CLASSIFICATION OF THIS PAGE	19. SECURITY CLASSIFICATION OF ABSTRACT	20. LIMITATION OF ABSTRACT
UNCLASSIFIED	UNCLASSIFIED	UNCLASSIFIED	

GENERAL INSTRUCTIONS FOR COMPLETING SF 298

The Report Documentation Page (RDP) is used in announcing and cataloging reports. It is important that this information be consistent with the rest of the report, particularly the cover and title page. Instructions for filling in each block of the form follow. It is important to ***stay within the lines*** to meet ***optical scanning requirements***.

Block 1. Agency Use Only *(Leave blank)*.

Block 2. Report Date. Full publication date including day, month, and year, if available (e.g. 1 Jan 88). Must cite at least the year.

Block 3. Type of Report and Dates Covered. State whether report is interim, final, etc. If applicable, enter inclusive report dates (e.g. 10 Jun 87 - 30 Jun 88).

Block 4. Title and Subtitle. A title is taken from the part of the report that provides the most meaningful and complete information. When a report is prepared in more than one volume, repeat the primary title, add volume number, and include subtitle for the specific volume. On classified documents enter the title classification in parentheses.

Block 5. Funding Numbers. To include contract and grant numbers; may include program element number(s), project number(s), task number(s), and work unit number(s). Use the following labels:

C	- Contract	**PR**	- Project
G	- Grant	**TA**	- Task
PE	- Program Element	**WU**	- Work Unit Accession No.

Block 6. Author(s). Name(s) of person(s) responsible for writing the report, performing the research, or credited with the content of the report. If editor or compiler, this should follow the name(s).

Block 7. Performing Organization Name(s) and Address(es). Self-explanatory.

Block 8. Performing Organization Report Number. Enter the unique alphanumeric report number(s) assigned by the organization performing the report.

Block 9. Sponsoring/Monitoring Agency Name(s) and Address(es). Self-explanatory.

Block 10. Sponsoring/Monitoring Agency Report Number. *(If known)*

Block 11. Supplementary Notes. Enter information not included elsewhere such as: Prepared in cooperation with ...; Trans. of ...; To be published in .... When a report is revised, include a statement whether the new report supersedes or supplements the older report.

Block 12a. Distribution/Availability Statement. Denotes public availability or limitations. Cite any availability to the public. Enter additional limitations or special markings in all capitals (e.g. NOFORN, REL, ITAR).

DOD	- See DoDD 5230.24, "Distribution Statements on Technical Documents."
DOE	- See authorities.
NASA	- See Handbook NHB 2200.2.
NTIS	- Leave blank.

Block 12b. Distribution Code.

DOD	- Leave blank.
DOE	- Enter DOE distribution categories from the Standard Distribution for Unclassified Scientific and Technical Reports.
NASA	- Leave blank.
NTIS	- Leave blank.

Block 13. Abstract. Include a brief *(Maximum 200 words)* factual summary of the most significant information contained in the report.

Block 14. Subject Terms. Keywords or phrases identifying major subjects in the report.

Block 15. Number of Pages. Enter the total number of pages.

Block 16. Price Code. Enter appropriate price code *(NTIS only)*.

Blocks 17. - 19. Security Classifications. Self-explanatory. Enter U.S. Security Classification in accordance with U.S. Security Regulations (i.e., UNCLASSIFIED). If form contains classified information, stamp classification on the top and bottom of the page.

Block 20. Limitation of Abstract. This block must be completed to assign a limitation to the abstract. Enter either UL (unlimited) or SAR (same as report). An entry in this block is necessary if the abstract is to be limited. If blank, the abstract is assumed to be unlimited.

COMPARISON OF STATION-KEEPING ALGORITHMS FOR AN INTERIOR LIBRATION POINT ORBIT IN THE SUN-EARTH+MOON ELLIPTIC RESTRICTED THREE-BODY PROBLEM

Lieutenant Colonel Steven C. Gordon,

Assistant Professor

Department of Mathematical Sciences

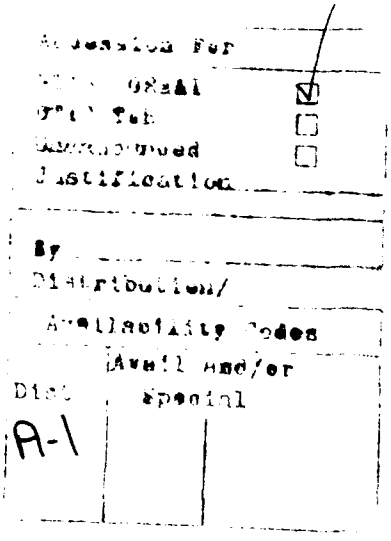

PREFACE

Bounded nominal paths can be constructed in the vicinity of the interior equilibrium point (sometimes called a libration or Lagrange point) for the Sun-Earth+Moon Elliptic Restricted Three-Body Problem. Numerical integration is used to generate the periodic or quasi-periodic reference trajectories in this effort, and the numerical data is then curve fit using a cubic spline routine. The force model used in this effort includes solar radiation pressure, the gravitational attractions of the Sun and the Earth+Moon barycenter, and the centrifugal force associated with rotation of the system. A spacecraft near a libration point orbit between the Earth and the Sun can study the interaction of the Sun's corona with the terrestrial environment and will thus be of great scientific value.

The spacecraft will, however, drift from the nominal path, and the forces affecting the spacecraft orbit have differing levels of uncertainty. Both range and range-rate tracking also include inaccuracy in the measurement. The accumulated error in the spacecraft's position and velocity relative to the nominal path after a predetermined period of tracking can be computed. This error, or uncertainty, in the spacecraft state is measured through simulations, commonly referred to as orbit determination error analysis, and is presented as either variances or standard deviations of the state vector elements.

The state uncertainty computed in the error analysis can then be input to a station-keeping algorithm. The algorithm computes control manuevers that return the spacecraft to the vicinity of the nominal (unstable) path. A control algorithm is required for an interior libration point orbit, and variations in orbital shapes and sizes may have some effect on the station-keeping costs. Several algorithms are derived and are used to test differences in station-keeping costs.

This effort is supported by the Frank J. Seiler Research Laboratory and has been conducted as doctoral research under the direction of Professor K.C. Howell, School of Aeronautics and Astronautics, Purdue University, West Lafayette, Indiana.

TABLE OF CONTENTS

LIST OF FIGURES

LIST OF TABLES

Table Page

INTRODUCTION

With the expansion of space exploration programs worldwide, interest has increased in the design of innovative, complex, and yet low-cost spacecraft trajectories that meet demanding mission requirements. In most of the missions flown in the last few decades, the spacecraft spent the majority of the flight time in a force environment dominated by a single gravitational field. For the preliminary mission analysis in these cases, additional attracting bodies and other forces could be modeled, when required, as perturbing influences. Analysis of some recently proposed and more adventurous missions, such as those involving libration point orbits, will require dynamic models of higher complexity, since at least two gravitational fields are of nearly equal influence on the spacecraft throughout the majority of the mission. Thus, trajectories determined for a system consisting of numerous gravitational forces have been of particular theoretical and practical interest in recent years.

One type of many-body problem, motion within a three-body system of forces, has a wide range of applications. The general problem of three bodies assumes that each body has finite mass and that the motion is a result of mutual gravitational attraction. When the mass of one of the three bodies is assumed to be sufficiently small (infinitesimal) so that it does not affect the motion of the other two bodies (primaries) in the system, the "restricted three-body problem" results. The primaries can be further assumed to be moving in known elliptic or circular orbits about their common center of mass. Therefore, the elliptic restricted three-body problem, where the primaries are assumed to be in known elliptic orbits, may be considered a reasonably approximate model for a spacecraft moving within the gravitational fields of the Sun and the Earth, for instance.

In the formulation of the restricted three-body problem, one mass is defined as infinitesimal relative to the remaining two masses (primaries). The primaries, unaffected by the infinitesimal mass, move under their mutual gravitational attractions. In the elliptic restricted three-body problem (ER3BP), the primaries are assumed to move on elliptic paths. If the eccentricity of the primaries' orbit is assumed to be zero, the circular restricted three-body problem (CR3BP) results. Even for known primary motion, however, a general, closed-form solution for motion of the third body of infinitesimal mass does not exist. In the restricted three-body problem (ER3BP or CR3BP), five equilibrium (libration) solutions can be found. These equilibrium points, sometimes called Lagrange points, are particular solutions of the equations of motion governing the path of the infinitesimal mass moving within the gravitational fields of the primaries.

The equilibrium points are defined relative to a coordinate system rotating with the primaries. At these locations, the forces on the spacecraft are in equilibrium. These forces include the gravitational forces from the massive bodies and the centrifugal force associated with the rotation of the system. (The addition of solar radiation pressure to the force model changes the locations of the five Lagrange points, although they can still be defined, and these solar radiation effects are discussed in Gordon[1].) The libration points are located in the plane of primary rotation. Three of the libration points are on the line between the two massive bodies, and one of these collinear points is interior to the primaries. The last two points are at the vertices of two equilateral triangles in the plane of primary rotation. The triangles have a common base that is the line between the primary masses.

For the CR3BP, the five libration points are stationary relative to the rotating reference frame. If the problem is generalized to the ER3BP, the libration points pulsate as the distance between the primaries varies with time. In both the circular and elliptic restricted problems, two-dimensional and three-dimensional trajectories, both periodic and quasi-periodic paths, can be computed in the vicinity of these libration points.

Three-dimensional, periodic "halo" orbits in the vicinity of the collinear libration points have been studied since the late 1960s. Early work concerning these orbits was motivated by studies related to exploring the far side of the Moon. These studies were completed in support of the planned Apollo 18 lunar exploration mission that was later canceled. Robert Farquhar coined the term "halo" to describe a three-dimensional, periodic orbit near a libration point on the far side of the Moon in the Earth-Moon system.[2] These orbits were designed to be large enough so that the spacecraft would be constantly in view of the Earth and would thus appear as a halo around the Moon. A communications station in this type of orbit could maintain constant contact between the Earth and a lunar experimentation station on the far side of the Moon.[3]

Quasi-periodic orbits near libration points are also currently of great research interest. The variations in size and shape that a quasi-periodic orbit can exhibit may add valuable flexibility for mission planning. This type of bounded, three-dimensional libration point trajectory is called a Lissajous orbit since specific planar projections of these quasi-periodic trajectories may look like a special type of "Lissajous" curve. Physicist Jules Antoine Lissajous (1822-1880) investigated curves that were generated by compounding simple harmonic motions at right angles, and he delivered a paper on this subject to the Paris Academy of Sciences in 1857. Nathaniel Bowditch of Salem, Massachusetts, had conducted some similar work in 1815. Lissajous curves have a wide variety of shapes that depend on the frequency, phase, and amplitude of the orthogonal components of the motion.[4,5] When the in-plane and the (orthogonal) out-of-plane frequencies of the linearized motion are nearly (but not) equal, the resulting path is typically called a Lissajous trajectory.

A method to generate approximations for this type of quasi-periodic orbital path was developed analytically by Farquhar and Kamel in 1973.[6] They derived a third-order approximate analytic solution for a translunar libration point orbit in the Earth-Moon ER3BP that also included solar gravity perturbations. In 1975, Richardson and Cary then developed a fourth-order analytic Lissajous approximation in the Sun-Earth+Moon barycenter system.[7] The notation "Earth+Moon"

indicates that the Earth and the Moon are treated as one body with mass center at the Earth-Moon barycenter. In consideration of the lunar perturbation, Farquhar has shown that the accuracy of solutions in the Sun-Earth CR3BP can be enhanced if the collinear libration points are defined along the line between the Sun and the center of mass of the Earth and the Moon.[8] Since 1975, a few researchers have considered methods to numerically generate Lissajous trajectories, but the lack of periodicity of a Lissajous path complicates numerical construction of bounded trajectories. Howell and Pernicka have developed a numerical technique for determination of three-dimensional, bounded Lissajous trajectories of arbitrary size and duration.[9-14] Orbits computed with their method are used in this effort to define the nominal path near which the spacecraft will be maintained.

Trajectory determination for a spacecraft that moves under the influence of a two-body system of forces will, however, be affected by many sources of error, including tracking errors, modeling uncertainty, and, possibly, control input errors. Orbit determination error analysis seeks to quantify the impact of the numerous errors that affect the motion of the spacecraft. The result of the error analysis is a determination of the spacecraft position and velocity uncertainty after some predetermined period of flight during which the spacecraft is affected by both the uncertainties in the forces and the errors in tracking data. The combined magnitude of the errors may be found to vary depending on the size and shape of the spacecraft orbit. A reduction in, or a more accurate estimation of, the magnitudes of the individual errors may be possible and could then lead to a significant reduction in overall vehicle position and velocity uncertainty.

This reduced level of position and velocity uncertainty may, in turn, reduce orbital "maintenance" costs, such as the propellant required to keep the spacecraft near the nominal orbit. The orbital maintenance routine is referred to here as "station-keeping." This cost is, in part, dependent on the accuracy of the tracking information because position updates using inaccurate tracking data may result in inefficient use of control energy and may also lead to unacceptable spacecraft drift from the nominal path. Other error sources may also

affect spacecraft drift from the (unstable) reference trajectory and, therefore, may increase station-keeping costs.

This research is concerned with developing and evaluating station-keeping algorithms for libration point orbits. The errors derived in orbit determination error analysis studies are used as random inputs in Monte Carlo simulations of the competing station-keeping algorithms. Other random inputs include solar radiation pressure uncertainty and control input errors. The output of the station-keeping trials is a function of the several random inputs and is consequently treated as a random variable. Statistical goodness of fit tests and equivalence of means and variances tests can then be appropriately conducted. The results associated with orbits designed to be periodic and quasi-periodic orbits are also compared. Chapter 1 briefly summarizes the background of the elliptic restricted three-body problem. Chapter 2 then derives several station-keeping methods, and, finally, Chapter 3 covers the results obtained.

CHAPTER 1: BACKGROUND

In this chapter, the elliptic restricted three-body problem and the associated coordinate systems are reviewed; the equations of motion for an infinitesimal mass moving in the gravity fields of two massive bodies are then presented. Next, locations of the libration points are discussed. The state transition matrix and the construction of bounded nominal orbits near the collinear Lagrange points are then summarized. Finally, curve fitting the nominal trajectory is covered. A more thorough discussion of these topics is presented in Gordon.[1,15]

A. Elliptic Restricted Three-Body Problem

The elliptic restricted three-body problem is a simplification of the general problem of three bodies. In the general three-body problem, each of the three bodies is assumed to be a particle of finite mass and, thus, exerts an influence on the motion of each of the other bodies. Neither the general nor the restricted problem of three bodies has a general closed-form solution. However, when problem simplifications are made, particular solutions can be determined. If the mass of one of the bodies is restricted to be infinitesimal, such that it does not affect the motion of the other two massive bodies (primaries), the restricted three-body model results. The primaries are assumed to be in known elliptic (ER3BP) or circular (CR3BP) orbits about their common mass center (barycenter). The problem can then be completely described by a single second-order vector differential equation with variables appropriately defined for a specified coordinate frame.

B. Coordinate Systems

The two standard coordinate systems used in the analysis of this problem have a common origin at the center of mass (barycenter) of the primaries. Primaries with masses m_1 and m_2 such that $m_1 \geq m_2$ are assumed here, although this distinction is arbitrary. The infinitesimal mass is denoted as m_3. These masses (m_1, m_2, m_3) correspond to particles situated at points P_1, P_2, and P_3, respectively. The barycenter is denoted as "B," and the resulting arrangement is shown in Figure 1-1. The rotating coordinate system is defined as $x_R y_R z_R$, and the inertial system is identified as $x_I y_I z_I$. Note that both coordinate systems are right-handed, and the x and y axes for both systems are in the plane of motion of the primaries. The x_I axis is, of course, assumed to be oriented in some fixed direction; in this specific formulation of the problem, it is assumed to be parallel to a vector defined with a base point at the Sun and directed toward periapsis of the Earth's orbit. The rotating x_R axis is defined along the line that joins the primaries and is directed from the larger toward the smaller primary. The z axes are coincident and are directed parallel to the primary system angular momentum vector. The y_I and y_R axes complete the right-handed $x_I y_I z_I$ and $x_R y_R z_R$ systems, respectively.

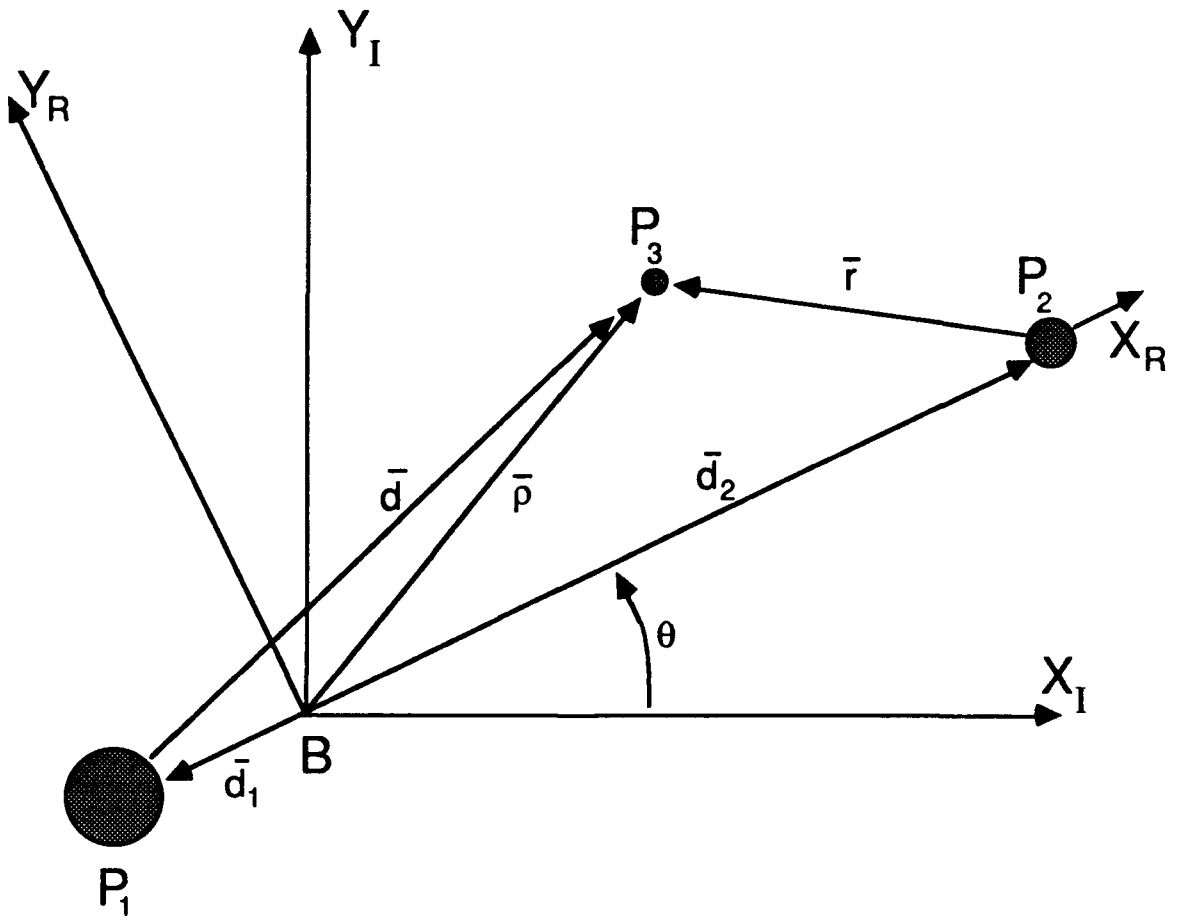

Figure 1-1. Coordinate Systems With Barycenter Origin.

C. Equations of Motion

Newtonian mechanics are used to formulate the equations of motion for m_3 (the spacecraft) relative to B as observed in the inertial reference frame. The sum of the forces on m_3 resulting from both the gravity fields of masses m_1 (the Sun) and m_2 (the Earth-Moon barycenter) and from the solar radiation pressure can be used to produce the following second-order vector differential equation:

$$\bar{\rho}'' = - G \left(\frac{m_1}{d^3}\right) \bar{d} - G \left(\frac{m_2}{r^3}\right) \bar{r} + \left(\frac{kS}{d^3}\right) \bar{d}. \qquad (1\text{-}1)$$

The overbar denotes a vector, and primes indicate differentiation with respect to dimensional time. All quantities are dimensional, as appropriate, and the quantity "G" is the universal gravitiational constant. The scalars "d" and "r" in equation (1-1) denote the magnitudes of the vectors $\bar{d}$ and $\bar{r}$, respectively, as depicted in Figure 1-1. The dimensionless scalar "k" is the solar reflectivity constant, and "S" is the solar radiation pressure constant. The formulation of the solar radiation force model and the values for the solar radiation constants are derived from previous work by Bell.[16] The values of the constants are described in Gordon.[1]

The position vector $\bar{\rho}$ is written in rotating components as

$$\bar{\rho} = x \hat{x}_R + y \hat{y}_R + z \hat{z}_R \qquad (1\text{-}2)$$

where $\hat{x}_R, \hat{y}_R, \hat{z}_R$ are unit vectors. The velocity and the acceleration of the spacecraft (particle P_3 with mass m_3) relative to the barycenter B as observed in the inertial reference frame can then be described. The following kinematic expression for $\bar{\rho}''$ can be derived:

$$\bar{\rho}'' = (x''-\theta''y-2\theta'y'-\theta'^2x)\hat{x}_R+(y''+\theta''x+2\theta'x'-\theta'^2y)\hat{y}_R+z''\hat{z}_R. \quad (1\text{-}3)$$

Three scaled equations of motion for P_3 can be derived using the the following scaling factors:

(1) The sum of the masses of the primaries equals one mass unit.

(2) The mean distance between the primaries equals one unit of distance.

(3) The universal gravitational constant is equal to one unit by proper choice of characteristic time.

The dimensional equations of motion can be simplified and scaled by introducing the characteristic quantities defined above and by introducing the nondimensional mass ratio μ, "psuedo-potential" U, and the scaled solar radiation constant s:

$$\mu = \frac{m_2}{m_1 + m_2} \quad (1\text{-}4)$$

and

$$U = \frac{(1-\mu)}{d} + \frac{\mu}{r} + \frac{1}{2}\dot{\theta}^2(x^2 + y^2) - \frac{k\,s}{d} \quad (1\text{-}5)$$

where the dot denotes the derivative with respect to characteristic time. The scaled solar radiation constant, s, is derived by using the characteristic quantities described above. Then, the vector magnitudes, "d" and "r," are written in terms of scaled quantities as:

$$d = [(x + \mu R)^2 + y^2 + z^2]^{1/2}, \tag{1-6}$$

$$r = [(x - R + \mu R)^2 + y^2 + z^2]^{1/2}. \tag{1-7}$$

The three scalar second-order differential equations that result can be written in terms of characteristic quantities as

$$\ddot{x} - 2\dot{\theta}\dot{y} = \frac{\partial U}{\partial x} + \ddot{\theta} y = U_x + \ddot{\theta} y, \tag{1-8}$$

$$\ddot{y} + 2\dot{\theta}\dot{x} = \frac{\partial U}{\partial y} - \ddot{\theta} x = U_y - \ddot{\theta} x, \tag{1-9}$$

$$\ddot{z} = \frac{\partial U}{\partial z} = U_z. \tag{1-10}$$

If the primaries are assumed to be moving in a circular orbit, equations (1-8), (1-9), and (1-10) reduce to three scalar equations in the simplified form:

$$\ddot{x} - 2\dot{y} = \frac{\partial U}{\partial x} = U_x, \tag{1-11}$$

$$\ddot{y} + 2\dot{x} = \frac{\partial U}{\partial y} = U_y, \tag{1-12}$$

$$\ddot{z} = \frac{\partial U}{\partial z} = U_z. \tag{1-13}$$

The scalar equations can be used to locate the five libration points in the rotating reference frame.

D. Locations of the Lagrangian Points

By using scalar equations (1-11), (1-12), and (1-13) for motion in the CR3BP, the locations of the stationary equilibrium points can be determined. Equations (1-8), (1-9), and (1-10) can be used to determine ratios of distances that are constant in the ER3BP; these ratios are related to the locations of libration points that have been defined in the ER3BP and that "pulsate" with respect to the rotating reference frame as the distance between the primaries varies with time.

1. The CR3BP

In the CR3BP, the five libration points are equilibrium points and are stationary with respect to the rotating coordinate frame, that is, they are locations at which the forces on the third body sum to zero. The arrangement of points and the corresponding nondimensional distances are depicted in Figure 1-2. Note that three of the libration points (L_1, L_2, L_3) are collinear with the primaries; one collinear

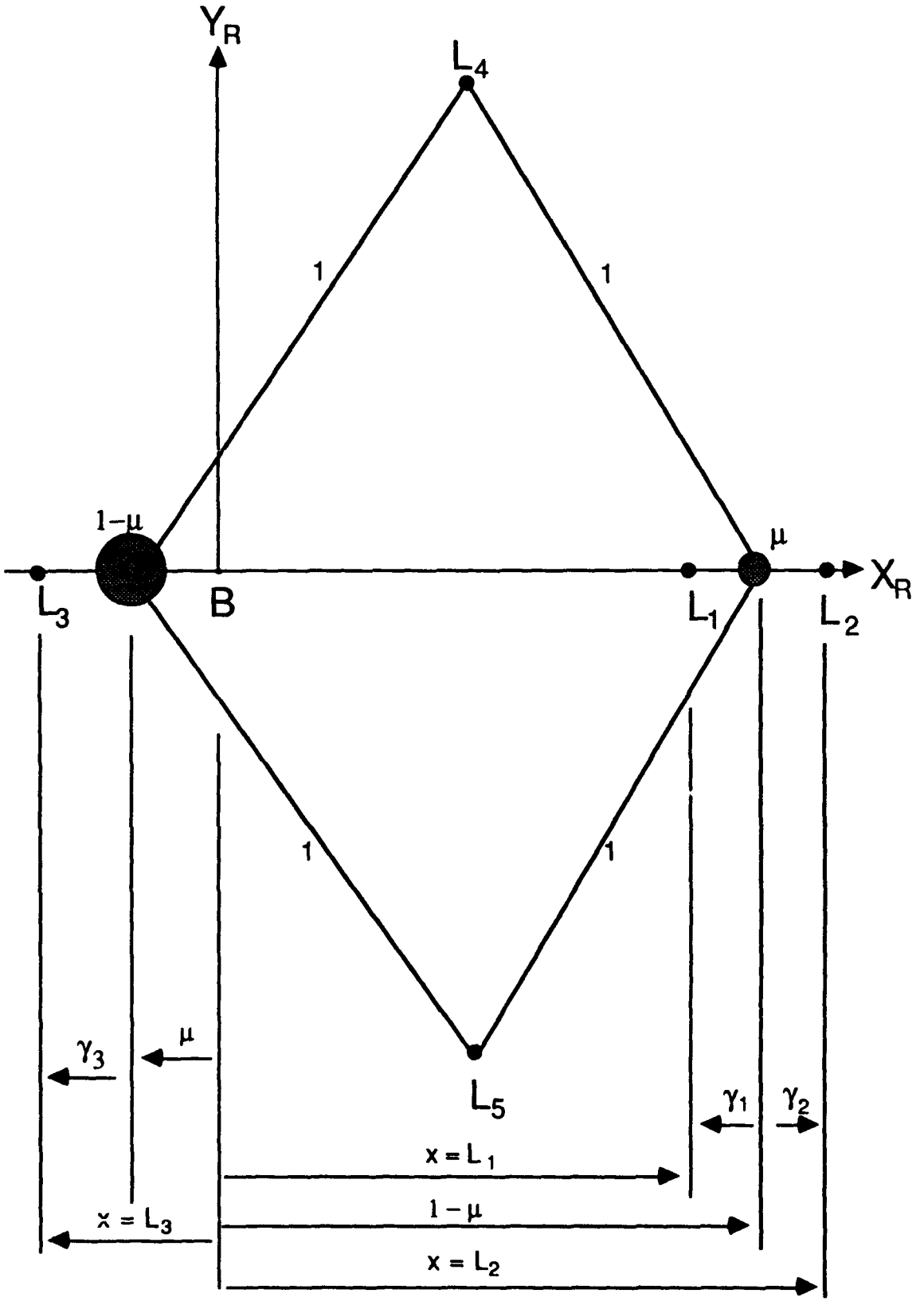

Figure 1-2. Lagrange Point Locations in the Scaled CR3BP.

point (L_1) is interior to the primaries. The remaining two points (L_4 and L_5) are located at the vertices of two equilateral triangles that are in the plane of primary rotation and that have a common base between the primaries.

In the CR3BP, the libration points are stationary in the rotating coordinate frame. Stationary points are defined as points at which the relative velocity and acceleration are zero, such that

$$\dot{x} = \dot{y} = \dot{z} = \ddot{x} = \ddot{y} = \ddot{z} = 0. \tag{1-14}$$

By using equations (1-14) in equations (1-11) through (1-13), the useful conditions $U_x = U_y = U_z = 0$ are found. The three collinear libration points can be readily located by further noting that $y = z = 0$ for the points located on the rotating x_R axis.

2. The ER3BP

Five libration points also exist in the ER3BP, but they are not stationary relative to the rotating frame; rather, the collinear points pulsate along the x_R axis, and the triangular points pulsate relative to both the x_R and the y_R axes as the distance between the primaries varies with time. The equilibrium solutions can be located by using equations (1-8) through (1-10) to find ratios of certain distances that are, in fact, constant in the problem. The collinear libration points in the ER3BP can be found by assuming $\dot{x} \neq 0$, $x \neq 0$, and $\dot{y} = \ddot{y} = \dot{z} = \ddot{z} = y = z = 0$. The relative locations of the libration points in the ER3BP are depicted in Figure 1-3.

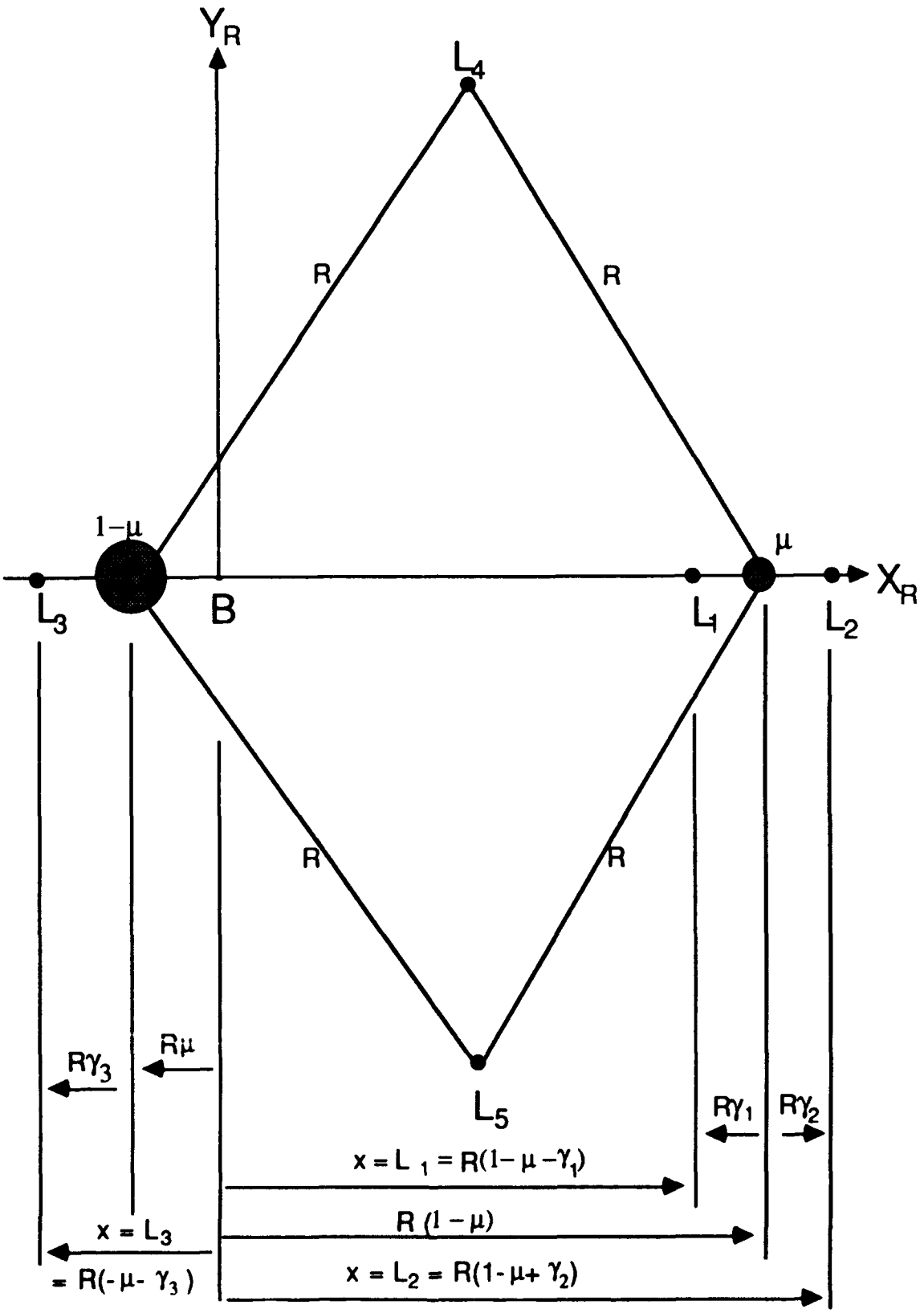

Figure 1-3. Lagrange Point Locations in the Scaled ER3BP.

E. State Transition Matrix

The state transition matrix is used in the calculation of the acceptable nominal trajectory, and it must also be available at varying time intervals along the nominal path for orbit determination error analysis investigations and station-keeping studies. The transition matrix is derived in connection with a linearizing analysis.

The equations of motion for the infinitesimal mass in the ER3BP can be linearized about a reference trajectory (nominal path) that is a solution of the differential equations. The states, three position and three velocity, and the state vector $\bar{x}$ are defined as

$$x_1 = x,\ x_2 = y,\ x_3 = z\ ,\ x_4 = \dot{x},\ x_5 = \dot{y},\ x_6 = \dot{z}, \tag{1-15}$$

and

$$\bar{x} = [x_1,\ x_2,\ x_3,\ x_4,\ x_5,\ x_6]^T. \tag{1-16}$$

The reference trajectory is defined as $\bar{x}_{REF}$. Therefore, using a Taylor's series approach, the expansion about the reference path is written in the form of the first-order variational equation

$$\frac{d}{dt}(\tilde{x}) = \dot{\tilde{x}} = A(t)\ \tilde{x} \tag{1-17}$$

where $\tilde{x} = \bar{x} - \bar{x}_{REF}$ is understood to be the vector of residuals relative to the nominal solution, and the matrix A(t) contains the first-order terms in the Taylor's series expansion of the equations of motion about the nominal or reference solution of interest.

Using equations (1-8) through (1-10), A(t) can be expressed as

$$A(t) = \begin{bmatrix} 0 & I \\ U_{rr}+\ddot{\theta}\Omega & 2\dot{\theta}\Omega \end{bmatrix} \tag{1-18}$$

where all four submatrices are dimension 3x3 and

$$U_{rr} = \begin{bmatrix} U_{xx} & U_{xy} & U_{xz} \\ U_{yx} & U_{yy} & U_{yz} \\ U_{zx} & U_{zy} & U_{zz} \end{bmatrix} \tag{1-19}$$

with

$$\Omega = \begin{bmatrix} 0 & 1 & 0 \\ -1 & 0 & 0 \\ 0 & 0 & 0 \end{bmatrix}.$$

In equation (1-19), the notation is simplified for the partial derivatives; for instance

$$\frac{\partial^2 U}{\partial x^2} = U_{xx}.$$

The matrix A(t) can then be evaluated along the reference trajectory.

The vector differential equation (1-17) governing the state variations from the nominal path has a solution of the form

$$\tilde{x}(t) = \Phi(t,t_0)\,\tilde{x}(t_0) \qquad (1\text{-}20)$$

where $\Phi(t,t_0)$ is the state transition matrix at time "t" relative to time "t_0." The matrix Φ, then, represents the sensitivities of the states at time "t" to small changes in the initial conditions. It is determined by numerically integrating the matrix differential equation

$$\frac{d}{dt}\Phi(t,t_0) = \dot{\Phi}(t,t_0) = A(t)\,\Phi(t,t_0), \qquad (1\text{-}21)$$

with initial conditions $\Phi(t_0,t_0) = I$, the 6x6 identity matrix. Thus, the nonlinear equations of motion in (1-8) through (1-10) and the matrix equation (1-21) combine to result in 42 first-order differential equations that can be simultaneously integrated numerically to determine the state vector and its associated transition matrix at any instant of time. The reference trajectories that are of interest in this research are generated by a numerical integration method that uses a differential corrections process developed by Howell and Pernicka.[9-14] The orbits include solar radiation pressure forces as formulated by Bell[16] specifically for an orbit associated with the interior Lagrange point in the Sun-Earth system. The numerical integration routines used in this work are fourth- and fifth-order Runge-Kutta formulas available in the 386-Matlab software package.[17]

F. Bounded Orbits Near Libration Points

The computation of bounded periodic and quasi-periodic orbits in the vicinity of libration points has been of increasing interest during the past 100 years. This section first discusses the stability of the libration points in the CR3BP and the ER3BP. The construction of bounded orbits near the collinear Lagrange points is then summarized.

Finally, the specific reference trajectories used in the orbit determination error analysis and station-keeping studies in this work are introduced.

1. Stability of the Libration Points in the CR3BP

The accomplishments of those researchers who have constructed bounded orbits near collinear libration points are particularly significant because the collinear points are considered "unstable" points of equilibrium but with (only) one mode producing positive exponential growth. Bounded motion in their vicinity, therefore, is determined by deliberately not exciting the unstable mode. A second mode produces negative exponential orbital decay and is also deliberately not excited. In the CR3BP, the remaining four eigenvalues are purely imaginary. The existence of initial conditions that result in only trigonometric (sinusoidal) functions as solutions means that the collinear libration points, while unstable, possess *conditional* stability (with proper choice of initial conditions) in the linear sense.[18]

The triangular libration points are marginally stable in the linear sense for a specific range of primary mass ratio in the CR3BP. Purely imaginary roots in two conjugate pairs are obtained for $\mu \leq .0385$, which is given here to four decimal places and is sometimes referred to as Routh's value.[19] The mass ratios (listed here to three decimal places), for example, in the three-body systems of the Earth-Moon ($\mu = 1.216 \times 10^{-6}$), Sun-Earth+Moon ($\mu = 3.022 \times 10^{-6}$) and Sun-Jupiter ($\mu = 9.485 \times 10^{-4}$) all satisfy the mass ratio requirement for marginal stability of the triangular points in the linearized model. Natural satellites, such as the Trojan asteroids or a moon of Saturn, occupy linearly stable orbits near triangular libration points in their respective systems.

2. Stability of the Libration Points in the ER3BP

Several researchers have analyzed the stability of the libration points in the elliptic problem, where both the mass ratio, μ, and the primary orbit eccentricity, e, influence stability.[18-22] The instability of the collinear libration points as determined in the circular problem for all the values of mass parameter persists for the elliptic problem; an analysis of the collinear points shows instability for any combination of the values of both μ and e.

The results of a linearized stability analysis regarding the effects of eccentricity and mass ratio on the linear stability of the triangular points have been published by Danby[21] and then later by Bennett[22]. Both Danby and Bennett have numerically generated graphic depictions of the linear stability region in the μ-e plane. For the eccentricity in the Sun-Earth+Moon ER3BP, the value of μ which ensures linear stability is only slightly less than Routh's value (decreased by approximately one percent). An interesting aspect of the μ-e stability region is that a range of values of μ greater than Routh's value also defines a region of linear stability for a specific range of values of e less than .3143.

3. Construction of Bounded Collinear Libration Point Orbits

The initial goal in the process of generating bounded orbits near a collinear (unstable) libration point is to avoid exciting the unstable mode associated with the linearized motion. The meteoric dust particles that may be orbiting near Lagrange point L_2 in the Sun-Earth system could only linger near that point if they arrive with the "correct" initial position and velocity states relative to L_2. The "correct" initial conditions will only (primarily) excite the stable modes associated with the linearized motion and not (or minimally) excite the unstable mode. The degree to which the unstable mode is excited will determine the length of time that the dust particles linger near L_2.

The third-order analytic representation is used in this work to provide the initial model for the trajectories. The method of successive approximations, using the linearized solution as the first approximation to the nonlinear orbital path, and the method of dual time scales are used to derive the third-order result.[6,7,23] The method of successive approximations is used to generate an asymptotic series in an appropriately small parameter. (The square root of the eccentricity of the primary orbit, that is the orbit of the Earth-Moon barycenter about the Sun, is the small parameter used here.) The method of dual time scales is used to convert the system of ordinary differential equations into a system of partial differential equations. In general, the method of multiple scales allows the various nonlinear resonance phenomena to be included in the approximate analytic solution and provides a method to remove secular terms. (Here, "secular" refers to terms that include the time variable and is derived from the French "siècle" meaning century.)

The analytic solution of Richardson and Cary[7] for the Sun-Earth+Moon ER3BP has been derived to fourth order, but the third-order approximation is found to be sufficient for this research.[9-14] A numerical integration algorithm, using a differential corrections procedure that is designed to adjust the first guess as obtained from the analytic approximation, can then be used to numerically generate the orbit of interest. A method developed by Howell and Pernicka[9-14] is used here to generate the orbital paths. Their method initially employs the approximate analytic solution to compute target points. A two-level (position matching then velocity matching), multi-step differential corrections algorithm is used to construct a numerically integrated, bounded trajectory that is continuous in position and velocity. A solar radiation pressure model developed by Bell[16] is also incorporated in the numerical integration procedure.

The method of Howell and Pernicka, including solar radiation pressure, uses an initial analytic guess that represents a halo orbit or, alternatively, a considerably smaller Lissajous path. The higher-order terms tend to slightly alter the first-order periodic or quasi-periodic path. Consequently, the initial target path for a halo orbit will generally not be precisely periodic. The two-level,

multi-step differential corrections procedure then adjusts the initial analytic target orbit and, therefore, will compute a halo-type orbit that is nearly (but not exactly) periodic.

4. The Reference Paths Generated for This Work

Precisely periodic halo orbits exist in the CR3BP. They also exist in the ER3BP, but, in the ER3BP, they are multiple revolution trajectories with periods much longer than those of interest here. Nearly periodic orbits are more practical in the ER3BP and are much more likely to be used in mission planning; therefore, the goal here should be slightly modified to be the comparison of Lissajous and "halo-type" orbits. The general shapes of the three-dimensional halo-type and Lissajous orbits can be seen by plotting three orthographic views of each orbit, using the tabular data from the numerical integration routine. Figure 1-4 depicts three orthographic views of point plots for the Lissajous orbit used in this research. Figure 1-5 contains three orthographic views (on a slightly different scale) of the considerably larger halo-type orbit. (Note that, in general, the amplitude ratio for Lissajous trajectories is arbitrary. In halo orbits, however, constraining the amplitude ratio results in equalized frequencies for in-plane and out-of-plane motion.) The orbits are depicted in the rotating reference frame centered at L_1.

Both orbits are clearly not periodic; a Lissajous orbit is often called a quasi-periodic path, and these two orbits could clearly be termed quasi-periodic or Lissajous paths. The major difference between the orbits is the larger size of the halo-type orbit; however, other differences are also present. The maximum x and y excursions of the halo-type orbit are approximately four times as large as those of the Lissajous path. Furthermore, the direction of motion (clockwise versus counterclockwise), as viewed in the y-z orthographic depiction, is different for the two orbits used here. The direction of motion on the halo-type orbit is counterclockwise in the y-z depiction; the direction of motion is clockwise in the y-z depiction for the Lissajous path. (Both orbits include clockwise motion in the x-y depiction.)

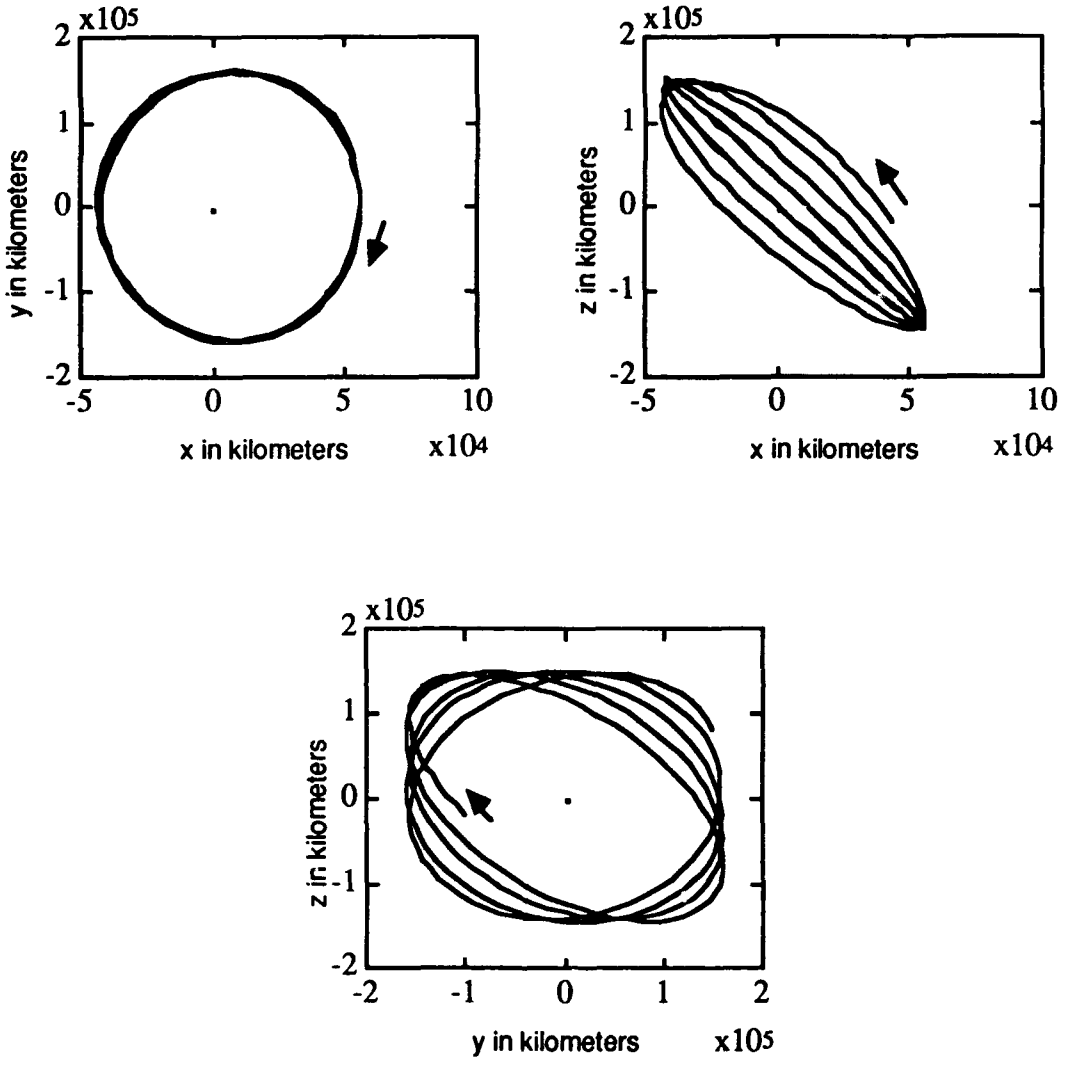

Indicates the direction of motion.

• Indicates the location of the libration point.

Figure 1-4. Three Orthographic Views of a Lissajous Orbit.

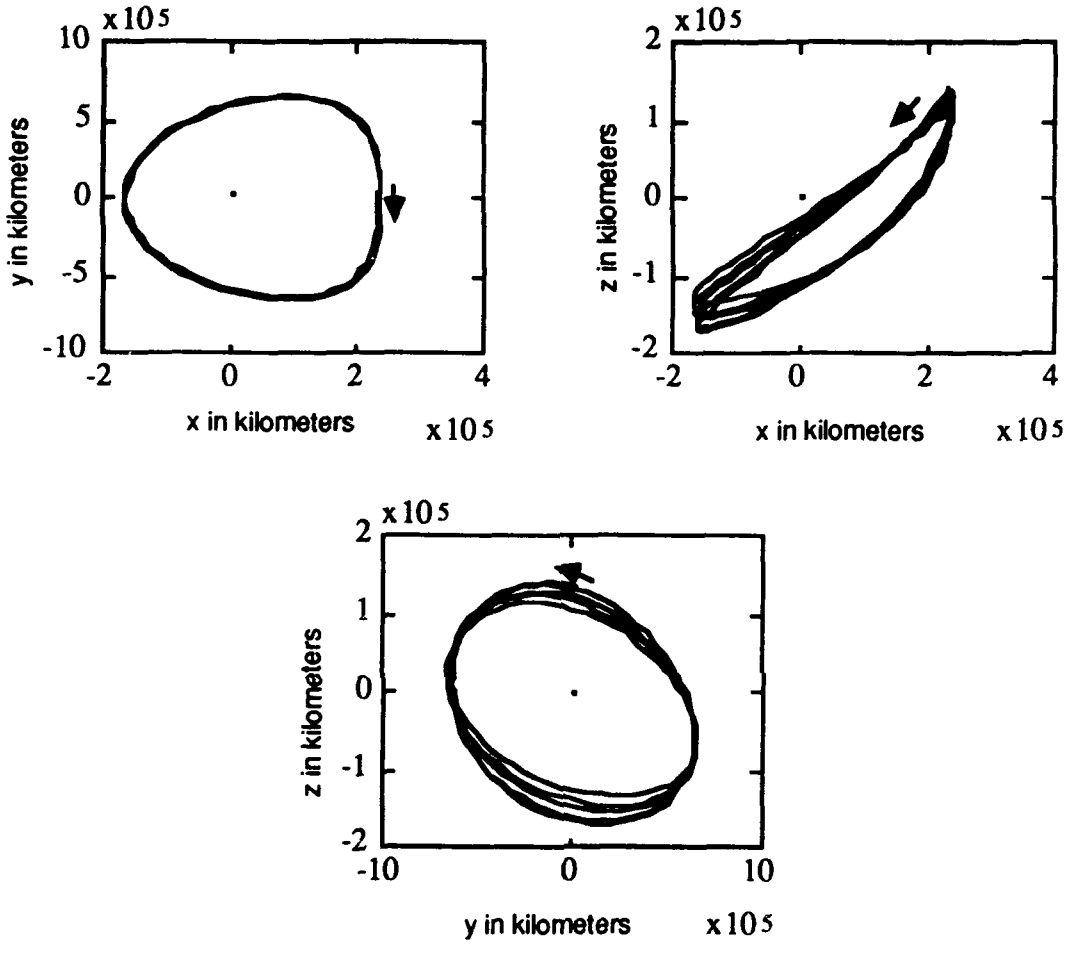

indicates direction of motion.

. indicates the libration point location.

Figure 1-5. Three Orthographic Views of a Halo-Type Orbit.

The two orbits can also be differentiated in terms of the direction of the maximum z excursion in the x-z depiction. If the maximum z excursion is in the positive z direction, the orbit can be termed a member of a "northern family" of orbits. When the maximum z excursion of the orbit is in the negative z direction, the orbit is termed a member of a "southern family" of orbits. In the x-z orthographic depiction, the smaller (Lissajous) path can be seen to be a member of a northern family of orbits, while the halo-type orbit is a member of a southern family of orbits.

Future work with these two orbits will include studies that generally require access to a nominal path that is at least piecewise smooth. Some method of curve fitting the numerically integrated data must consequently be investigated.

5. Curve Fitting the Nominal Path

The primary goal of this work is the completion of orbit determination error analysis for libration point trajectories. The conventional method for solution of state estimation problems, and the technique used in this effort, involves linearizing the nonlinear equations of motion about a reference solution (nominal path) and then applying linear estimation techniques. The orbit determination process is thus changed from estimating the state of a nonlinear system to estimating the linear, time-varying deviations from the reference trajectory.

The reference solution used in this research is generated by numerical integration of the nonlinear equations of motion. In one study, an investigation that used a consistent dynamic model for all comparisons, Richardson[8] has shown that a slight reduction in fuel expenditure can be realized if a numerically integrated, rather than an approximate analytic, nominal path is computed. The numerical integration method developed by Howell and Pernicka[9-14] is used here to generate a set of reference points for both position (three states) and velocity (three states), relative to the libration point of interest, at specified times. Time series point plots of all six state

variables for approximately a 2-year segment of a Lissajous orbit are depicted in Figures 1-6 (position states) and 1-7 (velocity states). The method computes numerical data for the six states in a reference frame that is centered at the libration point (in this case L_1) and that rotates with the primaries. However, the state estimation techniques and station-keeping algorithms used in this work require access to a continuous nominal path, rather than point plots, of acceptable accuracy.

The reference trajectory, represented as a (piecewise) smooth curve, could be constructed, approximately or exactly, through the points obtained from the numerical integration routine. The work here assumes that a curve that passes through the numerical data (exactly) is preferred. The effort required to generate a numerical solution, including forces modeled consistent with the ER3BP (or even more accurately modeled with ephemeris data) would seem to be wasted if the reference curve deviates too far from the numerical data. However, a method that approximates a smooth curve through the points is also desirable; that is, linear interpolation between the numerical data points was not considered acceptable. In one study, Pernicka[9] found that station-keeping costs for a libration point orbit were, in fact, sensitive to the accuracy of the curve fit. Clearly, a piecewise linear curve fit could not accurately match the concavity of the actual orbital path between data points, regardless of the size of the time steps used in the numerical integration routine.

Four methods of generating a curve for the nominal trajectory have been evaluated: Fourier series, least squares, weighted least squares, and cubic splines. The states associated with a quasi-periodic path were thought to be the most difficult to curve fit; therefore, various Lissajous trajectories were used to evaluate the curve-fitting methods. After several curve fitting evaluations, a cubic spline interpolation routine was selected to be used to model the reference trajectory in the state estimation simulations. The comparisons of the curve fit methods are fully described in Gordon.[15]

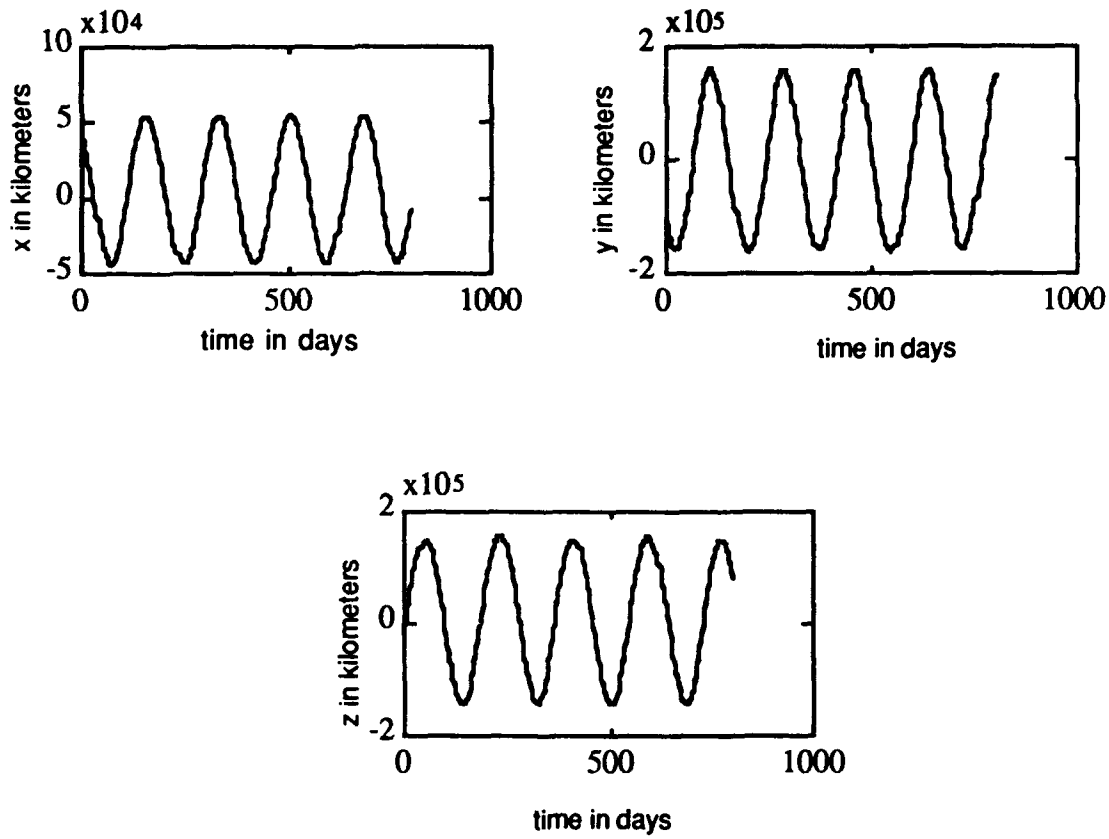

Figure 1-6. Time Series Plots of Three Lissajous Position States.

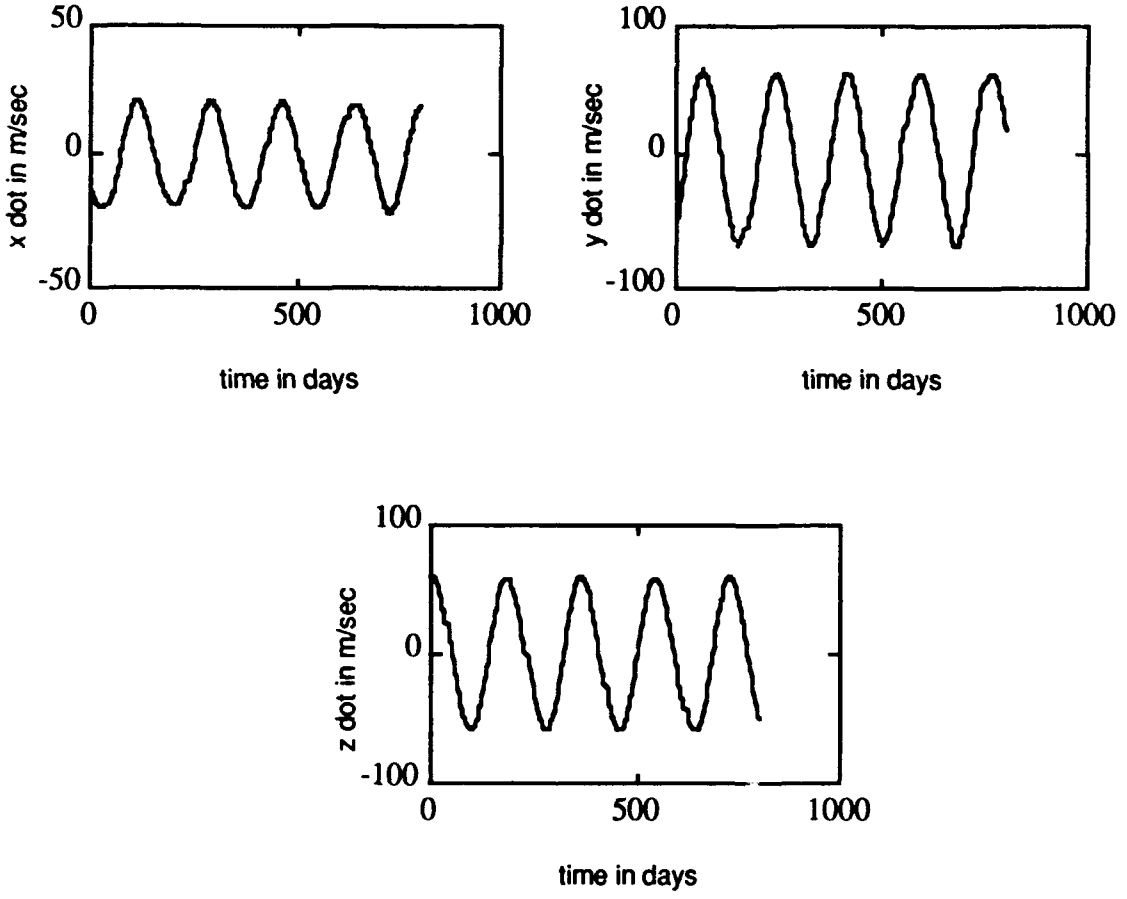

Figure 1-7. Time Series Plots of Three Lissajous Velocity States.

G. Orbit Determination Error Analysis Results

Complete, exact knowledge of the state of a spacecraft in orbit is generally not possible. Individual state variables cannot be measured precisely, and available measurements are usually some function of these state variables. For instance, a spacecraft moving along a libration point trajectory in the Sun-Earth system may be tracked using range and range-rate measurements containing random errors. The spacecraft may be affected by forces not included (or inadequately represented) in the dynamic model, and model parameters may be uncertain. By definition, the linearized system of equations used to model the nonlinear state variations is a further approximation. Also, actual control inputs may vary slightly in magnitude and direction from those commanded. These sources of error make knowledge of the spacecraft state uncertain. Computation of the most likely current state of the spacecraft in the presence of measurement and model uncertainty is the focus of orbit determination.

Error analysis involves an investigation of the impact of various sources of error on orbit determination. The output of an error analysis, as used in this work, provides the magnitudes of state vector variances and covariances, thus quantifying the relative contributions of the significant error sources. This output could then be used to predict how an improvement in measurement accuracy, for instance, would lessen state uncertainty. One benefit of more accurate knowledge of the state might be a reduction in station-keeping costs. A mathematical procedure can be developed to combine all information about the spacecraft state and filter this observed data based on the varying degrees of uncertainty. The filter then produces a "best estimate" of the state and additionally quantifies the resulting state variable uncertainties in preparation for an error analysis.

The orbit determination error analysis results can, in turn, be used in Monte Carlo simulations of competing station-keeping algorithms. The state error levels can be modeled as random errors with a specified mean and probability distribution. Of course, other error sources, such as solar radiation pressure uncertainty and control

input errors, can also be modeled in the Monte Carlo simulations. Gordon[24] discusses the evaluation of several orbit determination error analysis methods, uses hypothesis tests to determine the means and probability distributions of the errors, and computes the error levels appropriate for use in the station-keeping simulations. The state uncertainty levels are found to closely follow a zero-mean Gaussian distribution, and these state error levels are presented in Table 1 in terms of state element standard deviations.

Table 1. Error Levels Produced from Error Analysis Studies.

	One Standard Deviation Levels	
Coordinate	**Halo-Type Orbit**	**Lissajous Orbit**
x (km)	1.46	1.25
y (km)	2.64	3.35
z (km)	4.81	3.19
$\dot{x}$ (mm/sec)	1.40	1.25
$\dot{y}$ (mm/sec)	1.85	1.41
$\dot{z}$ (mm/sec)	2.49	2.51

CHAPTER TWO: STATION-KEEPING ALGORITHMS

Because of unavoidable errors, similar to those associated with any space mission, a station-keeping strategy is necessary to maintain the spacecraft within some predefined torus about the planned nominal path. The size and shape of the torus are determined by mission objectives including the possibly related requirements for orbit determination, scientific experimentation, and minimum fuel expenditure. For example, the nominal path may be computed to the highest degree of accuracy to meet both scientific specifications and tracking considerations. The size of the torus may then be tailored from "tight" to "loose" depending on mission objectives and comparisons of fuel expenditures for various options.

This chapter is organized into six sections. The first section contains an overview of the general station-keeping problem. The second section summarizes the derivations of two similar controllers, one of which has been used for libration point orbit station-keeping simulations. The next two sections summarize the derivations of two related control algorithms formulated for this work. Both of these station-keeping methods in the third and fourth sections are innovations on methods previously derived by Dwivedi[25,26] and Pernicka[9]. The fifth section contains a description of an on/off controller developed for this work.

The sixth and final section contains comparisons of the control costs derived from use of the station-keeping methods developed in this work for both a halo-type orbit as well as a more general Lissajous orbit. The comparisons require the use of statistical hypothesis tests similar to those used in the last section of chapter two. A station-keeping simulation will produce a scalar value for the total

propellant expended (Δv_T); also, each separate simulation will be subject to several random inputs and can, therefore, be considered a random trial. A group of random trials (station-keeping simulations) using consistent random inputs can then be treated as a random sample. The hypotheses tested in this final section pertain to the type of probability distribution that the random samples most closely follow and to equality of population variances and means.

A. Definition of the Station-Keeping Problem

Even for an accurate nominal trajectory, unmodeled as well as poorly modeled forces on the spacecraft will generally be present, and the resulting modeling errors may be a contributing cause of spacecraft drift from the nominal path. As was discussed in Chapter 1, a trajectory near a collinear libration point is designed to excite only the stable modes associated with the motion. When the spacecraft deviates from this nominal trajectory, the unstable mode may be excited, and drift from the path may then increase exponentially with time. A station-keeping method can thus be used to combat this drift and keep the spacecraft acceptably close to the nominal path. Of course, specifications associated with the station-keeping procedure will influence the deviations from the nominal path. For example, as the torus about the nominal path is relaxed or as the minimum acceptable separation time between control inputs is increased, drift from the nominal path may increase.

How large will the drift be? Table 2 contains the partial results from several numerical simulations and illustrates the magnitude and direction of spacecraft drift from a nominal halo path due to deterministic errors in initial conditions ("Δx") or solar reflectivity ("Δk"). For these simulations, the deterministic initial position errors are computed from a consistent position on the halo orbit. The units for position deviations are kilometers; the units for velocity deviations are in millimeters per second.

Table 2. Nominal Path Deviations due to Deterministic Errors. (The units for position are kilometers; velocity is in mm/sec.)

		Deviation from the Nominal Path after							
	Δx	20 days		40 days		60 days		80 days	
		Δk=0	Δk=.13	Δk=0	Δk=.13	Δk=0	Δk=.13	Δk=0	Δk=.13
x	1	4.5	14.6	11.9	59.0	-5.9	122.5	-59.4	242.5
y	1	1.5	-.6	-.9	-14.7	-12.5	-56.7	-35.6	-153.0
z	1	2.1	1.9	2.1	1.0	5.6	3.5	6.9	9.9
$\dot{x}$	1	3.3	15.8	6.8	38.5	-2.4	64.3	-28.4	116.7
$\dot{y}$	1	-.5	-3.8	-1.9	-13.0	-.9	-26.9	5.0	-61.5
$\dot{z}$	1	.1	-.2	-.8	-1.6	-.2	.1	-.5	6.4
x	1	38.6	138.2		316.2		677.0		
y	1	7.4	-16.8		-94.0		-286.2		
z	1	15.0	17.0		13.8		18.1		
$\dot{x}$	10	44.1	83.9		157.4		317.1		
$\dot{y}$	10	-4.2	-24.6		-58.9		-151.5		
$\dot{z}$	10	4.9	-3.2		-3.0		10.4		
x	1	278.2	930.2		2253.8		5025.0		
y	1	39.5	-37.7		-466.5		-1616.8		
z	1	42.6	177.8		116.7		100.5		
$\dot{x}$	100	81.7	538.0		1088.6		2324.1		
$\dot{y}$	100	-23.4	-141.2		-378.4		-1051.2		
$\dot{z}$	100	-18.5	-18.9		-43.5		503.2		
x	10	20.2	30.3	51.7	98.7	85.6	214.0	141.7	443.6
y	10	7.3	5.3	-3.9	-17.8	-33.6	-77.8	-100.6	-218.0
z	10	7.1	6.9	-1.9	-3.1	-6.3	-8.4	-4.4	-1.4
$\dot{x}$	1	11.6	24.1	27.1	58.9	39.8	106.5	63.1	208.3
$\dot{y}$	1	-4.0	-7.3	-9.0	-20.0	-16.1	-42.1	35.8	-102.3
$\dot{z}$	1	-4.3	-4.5	-6.3	-7.2	-3.1	-2.8	4.0	11.0

Table 2, continued.

		Deviation from the Nominal Path after							
	Δx	20 days		40 days		60 days		80 days	
		Δk=0	Δk=.13	Δk=0	Δk=.13	Δk=0	Δk=.13	Δk=0	Δk=.13
x	50	90.0	100.1	228.1	275.1	491.9	620.3	1035.4	1337.4
y	50	33.4	31.5	-17.5	-31.3	-127.1	-1[illegible].3	-389.6	-507.0
z	50	29.6	29.4	-19.8	-20.9	-59.2	-61.3	-54.6	-51.6
$\dot{x}$	1	48.4	60.9	117.5	149.3	227.4	294.1	470.0	615.3
$\dot{y}$	1	-19.7	-23.0	-40.3	-51.4	-83.5	-109.5	-217.2	-283.7
$\dot{z}$	1	-23.4	-23.7	-31.0	-31.8	-16.0	-15.7	24.5	31.4
x	50		124.2		354.3		814.1		1772.0
y	50		39.5		-33.4		-208.5		-640.1
z	50		42.6		-4.9		-51.0		-43.3
$\dot{x}$	10		81.7		194.7		387.2		815.8
$\dot{y}$	10		-23.4		-63.0		-141.5		-373.7
$\dot{z}$	10		-18.5		-33.4		-19.6		35.4
x	100	177.3	187.4	448.7	495.8	999.9	1128.4	2152.9	2455.0
y	100	66.2	64.2	-34.4	-48.2	-243.9	-288.1	750.7	-868.0
z	100	57.7	57.5	-42.1	-43.3	-125.3	-127.4	117.3	-114.3
$\dot{x}$	1	94.5	106.9	230.5	262.3	462.0	528.7	1000.0	1124.4
$\dot{y}$	1	-39.3	-42.6	-79.5	-90.5	-167.8	-193.8	-400.0	-510.4
$\dot{z}$	1	-47.3	-47.6	-61.8	-62.7	-32.0	-31.7	-100.0	57.1
x	200	351.7	361.9	890.0	937.0	2016.2	2144.7	4390.0	4691.8
y	200	131.6	129.5	-68.2	-82.0	-477.6	-521.7	-1472.3	-1589.6
z	200	1.1	113.6	-86.9	-88.0	-257.5	-259.6	-242.4	-239.4
$\dot{x}$	1	186.0	199.0	456.6	488.4	931.4	998.1	1998.6	2144.0
$\dot{y}$	1	-78.6	-81.9	-157.8	-168.9	-336.1	-362.1	-897.0	-963.4
$\dot{z}$	1	-95.1	-95.4	-234.8	-124.3	-64.2	-63.8	-101.6	1086.6

Notice that the magnitude of the drift is sensitive to both initial velocity and initial position deviations and that a solar reflectivity constant error of 13% also has a substantial effect on the drift. Of course, the drift will undoubtably vary, perhaps in a minor way, depending on the size and shape of the nominal orbit and the location on the path at which the deviations are evaluated. Clearly, however, a spacecraft can quickly move quite far from the nominal path.

One approach that might be considered for a station-keeping strategy is to redefine the nominal path such that it passes through the current position. (Some guidance procedures for interplanetary missions have successfully employed such a scheme.) Unfortunately, an additional complication associated with a libration point orbit is that a nominal path cannot generally be defined through all possible positions. A bounded orbit may not exist through an arbitrary point, and the computational difficulty required to construct a nominal orbit through an approximate set of coordinates also makes redefining the nominal path during flight virtually impossible. Therefore, a station-keeping algorithm that returns the spacecraft to a torus about the reference trajectory is essential.

A station-keeping strategy must combat the exhibited drift from the nominal path while satisfying some predetermined set of specifications. It is not uncommon for a station-keeping scheme to include constraints related to quantities such as the timing of manuevers, control magnitude, and deviation distance from the nominal path. (Of course, additional types of constraints have been implemented in other guidance schemes and could possibly prove beneficial in future libration point orbit studies.) Identifying a lower bound for such quantities may be necessary to allow time for orbit determination and to help ensure efficient use of control energy. Figure 2-1 illustrates the decision process necessary to implement the minimal restrictions typically used in the control algorithms developed in this chapter. Each of the decision steps depicted in Figure 2-1 may serve to delay the input of control force.

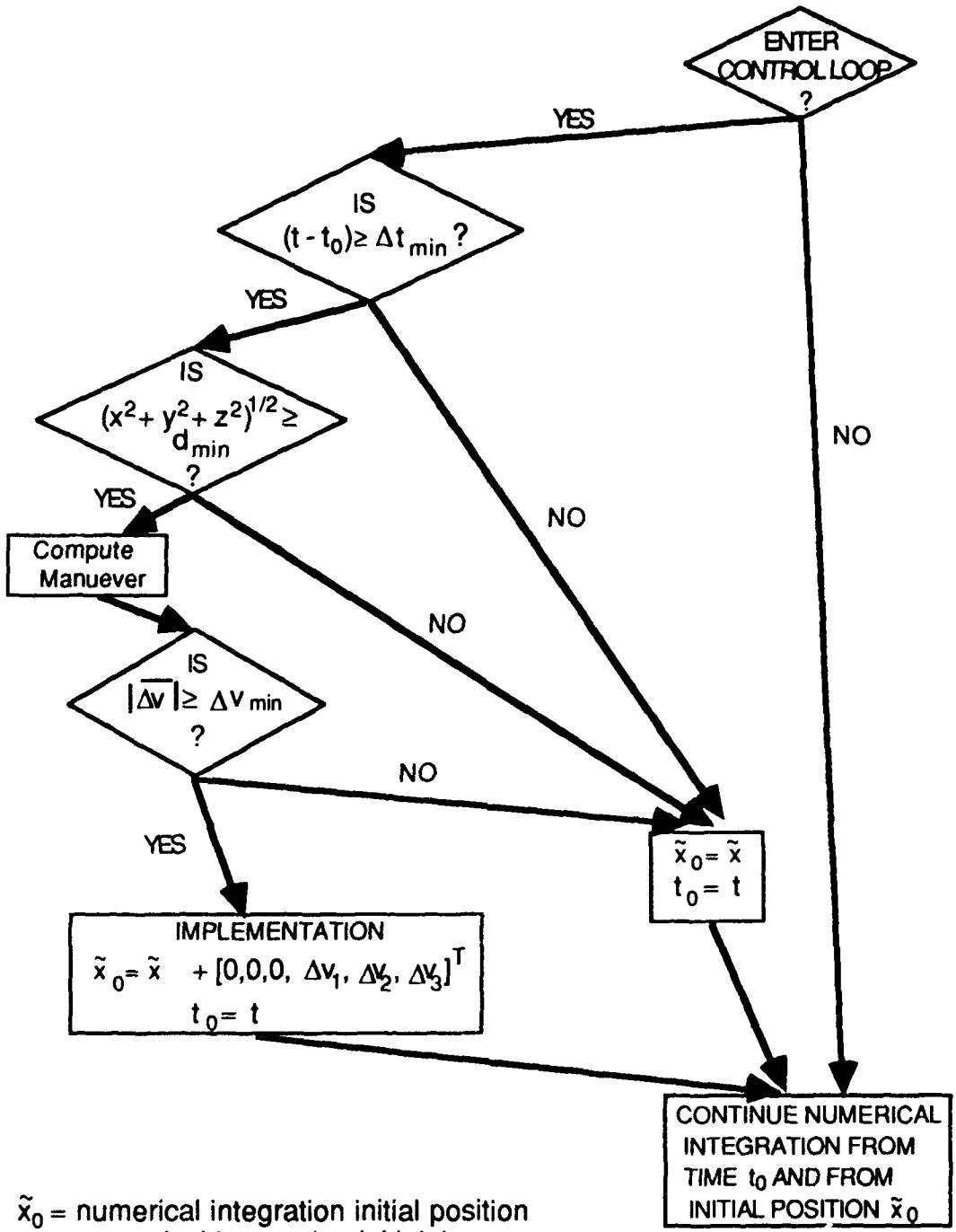

$\tilde{x}_0$ = numerical integration initial position
t_0 = numerical integration initial time
$\tilde{x}$ = current position of the spacecraft as the control loop is entered
t = current time when the control loop is entered
Δt_{min} = minimum control separation time
Δv_{min} = minimum control magnitude
d_{min} = minimum deviation magnitude from the nominal path

Figure 2-1. Decision Process for Control Inputs.

For a collinear libration point orbit, a small deviation from the (unstable) nominal trajectory can lead to rather large drift from the path in a short time. In effect, the station-keeping algorithm must combat both the current drift from the path in addition to the exponential increase in the drift that is expected if no correction is implemented. Any delay in the control actuation may allow the drift to increase and to thus compound the station-keeping problem. The magnitude of the drift can be clearly seen in Table 2. Of course, in such a nonlinear problem, it is possible for the spacecraft to begin returning to the nominal path on its own. Another possible constraint for the station-keeping scheme could be a check on the growth or decay of the drift. This check on the spacecraft's drift from the nominal path may serve to delay a control input, or it may prove efficient to input control energy at the current time to "assist" the drift back to the path. The optimal timing (now or at some future "best" time) to implement a given control input is a possible area for future research.

The goal of the station-keeping routine is then to keep the spacecraft "close enough" to the reference trajectory. The allowable deviations may depend on the simulation experience with a given control algorithm and on mission constraints, including the propellant cost that can be tolerated. The evaluation of various minimal restrictions is addressed in later sections. When the spacecraft is "near" the nominal trajectory, it is reasonable to model the deviations from the reference path using linear analysis. Consistent with such a model, an investigation of the problem incorporating *linear* control theory is thus initiated.

B. Previously Developed Station-Keeping Strategies

Early work by Dwivedi[25,26] resulted in development of a control procedure that is derived from minimization of a cost functional. His approach was developed for interplanetary space flight; however, it also shows promise as a controller for libration point orbits. The cost function is defined by weighting both the control energy used at an initial time and the expected deviations of the spacecraft from the

nominal path at two distinct times in the future. The points used to compute deviations from the nominal path are referred to in this work as "target points." These points are defined along the nominal path at predetermined times that are called "target times." (More than two target points can be used; this modification proves valuable later in this effort.) A version of Dwivedi's controller, using distinct manuever times, is summarized here, and an extended derivation used by Pernicka[9] is then also described.

In Dwivedi's algorithm, the cost function includes several submatrices partitioned from the state transition matrix. The state transition matrix is derived, in the usual way, through a linearizing process relative to the nominal path. For notational ease, the state transition matrix is partioned into four 3x3 submatrices as

$$\Phi(t_k, t_0) = \begin{bmatrix} A_{k0} & B_{k0} \\ C_{k0} & D_{k0} \end{bmatrix}. \qquad (2\text{-}1)$$

Dwivedi's controller, in this formulation, computes a $\overline{\Delta v}$ input (a 3x1 vector), with magnitude denoted as Δv, for a time denoted as t_0. The $\overline{\Delta v}$ is added to the initial velocity states in the numerical integration routine in order to change the deviation of the spacecraft from the nominal path at some future times. In this derivation, $\bar{m}_k$ is the position deviation (a 3x1 vector) and $\bar{v}_k$ is the velocity deviation (a 3x1 vector) of the spacecraft from the nominal path at time t_k, with k = 1, 2, etc. If $\bar{e}_0$ is the residual velocity (a 3x1 vector) and $\bar{p}_0$ is the residual position (a 3x1 vector) relative to the nominal path at time t_0, then a $\overline{\Delta v}$ input at t_0 could be used to predict $\bar{m}_k$ for k = 1, 2, etc. For instance, when the initial position $\tilde{x}_0$ includes an initial velocity perturbation $\bar{e}_0$, a delta velocity $\overline{\Delta v}$, and an initial position perturbation $\bar{p}_0$, the state propagation equation provides:[24]

$$\tilde{x}_k = \begin{bmatrix} \bar{m}_k \\ \bar{v}_k \end{bmatrix} = \Phi(t_k, t_0)\, \tilde{x}_0 = \Phi(t_k, t_0) \begin{bmatrix} \bar{p}_0 \\ \bar{e}_0 + \overline{\Delta v} \end{bmatrix}. \qquad (2\text{-}2)$$

As an example, for two target times t_1 and t_2, and by assuming that $\bar{p}_0$ is the zero vector,

$$\bar{m}_1 = B_{10}\bar{e}_0 + B_{10}\overline{\Delta v} \qquad (2\text{-}3)$$

and

$$\bar{m}_2 = B_{20}\bar{e}_0 + B_{20}\overline{\Delta v}. \qquad (2\text{-}4)$$

Dwivedi's approach was developed for application to interplanetary missions and, consequently, includes the assumption that position deviations from the nominal path have a minor effect on spacecraft drift when compared to velocity deviations. Hence, $\bar{p}_0$ is allowed to be the zero vector when deriving equations (2-3) and (2-4) from equation (2-2). The target times t_1 and t_2 are computed by adding incremental times Δt_1 and Δt_2 to t_0, respectively. For instance, if Δt_1 = 40 days, Δt_2 = 70 days, and t_0 = 0 days, then $t_1 = t_0 + \Delta t_1$ = 40 days and the second target time $t_2 = t_0 + \Delta t_2$ = 70 days.

The cost function that will be minimized is

$$J(\overline{\Delta v}) = \overline{\Delta v}^T Q\, \overline{\Delta v} + \bar{m}_1^T R\, \bar{m}_1 + \bar{m}_2^T S\, \bar{m}_2 \qquad (2\text{-}5)$$

where the weighting matrix Q is symmetric positive definite, and the weighting matrices R and S are positive semidefinite. Equation (2-5) can be written in terms $\overline{\Delta v}$ by substituting equations (2-3) and (2-4)

into equation (2-5). Figure 2-2 depicts a version of Dwivedi's station-keeping routine that allows the control input at a specified time other than t_0 and that uses two target times, which are actually incremental times Δt_1 and Δt_2 added to the initial time t_0.

Determination of the $\overline{\Delta v}$ corresponding to the relative minimum of this cost function allows a linear equation for the optimal control input ($\overline{\Delta v}^*$) to be found:[25,26]

$$\overline{\Delta v}^* = -[Q + B_{10}^T R\, B_{10} + B_{20}^T S\, B_{20}]^{-1}[B_{10}^T R\, B_{10} + B_{20}^T S\, B_{20}]\, \bar{e}_0. \qquad (2\text{-}6)$$

Note that equation (2-6) assumes control implementation at time t_0. This derivation could be generalized to include the possibility of time-varying weighting matrices and a $\overline{\Delta v}$ input at some time t after t_0, and these generalizations could be the subjects of valuable future research concerning libration point orbital control.

Howell and Pernicka[9,27] modified the above controller to also include the effects of position deviations at time t_0. Dwivedi's approach assumes that velocity perturbations have a much greater propagative effect than position deviations from the nominal path. Because of the unstable nature of libration point orbits, it was reasoned that both position and velocity residuals from the nominal path should be included in the error propagation equations such as equation (2-3) and equation (2-4) for Dwivedi's controller. An example of the relationship between position and velocity errors at t_0 and the resulting residuals at varying time steps later was illustrated in Table 2.

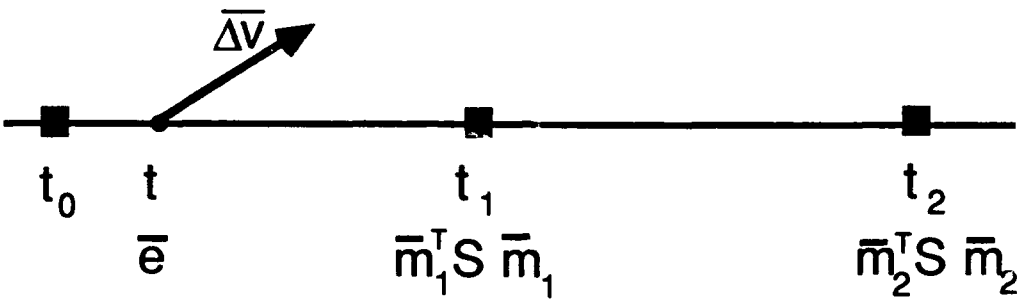

$\bar{e}$ = VELOCITY DEVIATION FROM THE NOMINAL PATH AT TIME t. THIS IS A 3 x 1 VECTOR.

$\bar{m}_1^T$= POSITION DEVIATION FROM THE NOMINAL PATH AT TIME t_1 IF $\overline{\Delta v}$ IS INPUT AT TIME t. THIS IS A 3 x 1 VECTOR.

$\bar{m}_2^T$= POSITION DEVIATION FROM THE NOMINAL PATH AT TIME t_2 IF $\overline{\Delta v}$ IS INPUT AT TIME t. THIS IS A 3 x 1 VECTOR.

R, S ARE 3 x 3 POSITIVE SEMIDEFINITE WEIGHTING MATRICES USED IN THE COST FUNCTION.

Figure 2-2. Dwivedi Control Routine.

Certainly, both position and velocity offsets from the nominal trajectory do appear to make a substantial contribution to spacecraft drift from the nominal path. For this derivation, $\bar{p}_0$ is the nonzero position residual vector (3x1) and $\bar{e}_0$ is again the nonzero velocity residual vector (3x1) at time t_0; by using equation (2-2), the following two equations can be derived:

$$\bar{m}_1 = B_{10}\bar{e}_0 + B_{10}\overline{\Delta v} + A_{10}\bar{p}_0 \tag{2-7}$$

$$\bar{m}_2 = B_{20}\bar{e}_0 + B_{20}\overline{\Delta v} + A_{20}\bar{p}_0. \tag{2-8}$$

Figure 2-3 is a depiction of the Howell/Pernicka controller that uses a control input at t_0 and also uses two target times (at predetermined incremental times beyond t_0). The cost function that is minimized remains as

$$J(\overline{\Delta v}) = \overline{\Delta v}^T Q\, \overline{\Delta v} + \bar{m}_1^T R\, \bar{m}_1 + \bar{m}_2^T S\, \bar{m}_2. \tag{2-9}$$

Using equations (2-7) and (2-8) in equation (2-9), the optimal control is obtained by minimizing the cost function in terms of $\overline{\Delta v}$, and it then becomes[9,27]

$$\overline{\Delta v}^* = -\,[\,Q + B_{10}^T R\, B_{10} + B_{20}^T S\, B_{20}]^{-1}[(B_{10}^T R\, B_{10} + B_{20}^T S\, B_{20})\,\bar{e}_0 +$$

$$(B_{10}^T R\, A_{10} + B_{20}^T S\, A_{20})\,\bar{p}_0]. \tag{2-10}$$

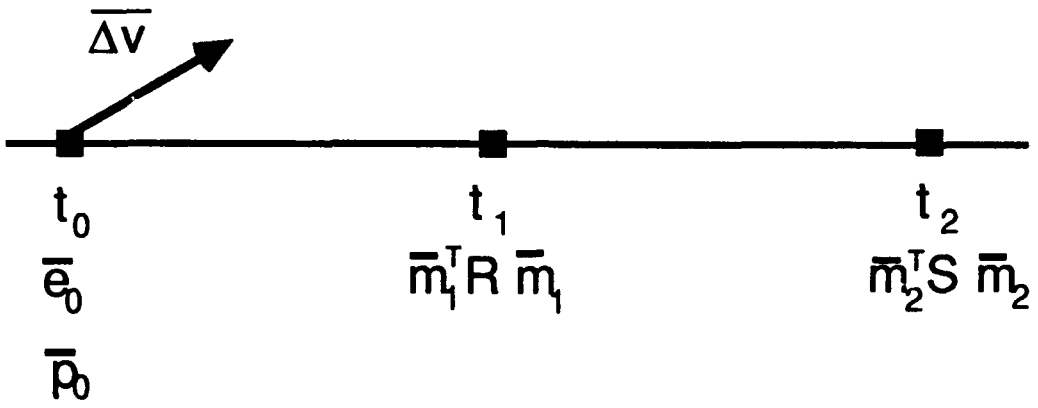

$\bar{e}_0$ = VELOCITY DEVIATION FROM THE NOMINAL PATH AT TIME t_0. THIS IS A 3 x 1 VECTOR.

$\bar{p}_0$ = POSITION DEVIATION FROM THE NOMINAL PATH AT TIME t_0. THIS IS A 3 x 1 VECTOR.

$\bar{m}_1$ = POSITION DEVIATION FROM THE NOMINAL PATH AT TIME t_1 IF $\overline{\Delta v}$ IS INPUT AT TIME t_0. THIS IS A 3 x 1 VECTOR.

$\bar{m}_2$ = POSITION DEVIATION FROM THE NOMINAL PATH AT TIME t_2 IF $\overline{\Delta v}$ IS INPUT AT TIME t_0. THIS IS A 3 x 1 VECTOR.

R, S ARE 3 x 3 POSITIVE SEMIDEFINITE WEIGHTING MATRICES USED IN THE COST FUNCTION.

Figure 2-3. Howell/Pernicka Control Scheme

Clearly, the Howell/Pernicka formula[9,27] for the optimal control input is slightly more complicated than that derived using Dwivedi's approach. The inclusion of the position deviation ($\bar{p}_0$) in equation (2-10), versus using equation (2-6), may be shown, in fact, to reduce the control costs. Both the Dwivedi and the Howell/Pernicka control algorithms can be used for quasi-periodic and periodic libration point orbits. Howell and Pernicka[9,27] used their control law (2-10) for a spacecraft in a halo-type orbit near the interior libration point in the Sun-Earth+Moon system, and their algorithm was formulated to include several features. Minimal separation times of up to 80 days between control inputs were used. This is a realistic feature because the orbit determination process and the control input computations require some minimal work time. The 80-day control separation time was selected to roughly correspond to the timing between manuevers used for ISEE-3. They also included a minimal control input ("Δv") magnitude in their formulation. Modern propellant devices do have restrictions concerning the minimal control energy that can be accurately expended, and the errors relative to the commanded control may be a function of the control magnitude. (In fact, the control uncertainty modeled later in the station-keeping simulations may be inversely related to control magnitude.) The values that Howell and Pernicka used for the minimal Δv ranged between .01 and .5 meters per second depending on the specific simulation completed.

Incorporating a torus of acceptable size about the nominal path is also a useful feature. Howell and Pernicka used a torus that ranged between 0 and 100 kilometers in radius. If the specific torus dimensions were not violated, even when all other conditions for a control input were met, no $\overline{\Delta v}$ would be expended. The control costs found in Howell and Pernicka[9,27] are generally comparable to those found in other investigations. (These results will be included in the last section of this chapter.) However, it is noted that simulations that included tracking and injection errors and a minimum control separation time of 80 days had relatively high propellant costs. These propellant costs are also obviously a function of the target point spacing; therefore, changes in specifications may enable some reduction

in the cost. It should also be noted that ISEE-3 was successfully controlled at a cost that was lower than the propellant cost predicted by pre-mission station-keeping simulations. Further investigation of the choices of weighting matrices (both constant and time-varying), the number of target points, and the target spacing may prove valuable; alternatively, a controller that also weights velocity residuals at the target times may prove to be an improvement.

C. Delta-Velocity Controller I

An innovation that also adds velocity residual weighting in the cost function of the Howell/Pernicka[9,27] controller provides promising results. For this controller, the velocity residuals at t_1 (denoted by $\bar{v}_1$) and t_2 (denoted by $\bar{v}_2$) are 3x1 vectors that can be computed as

$$\begin{bmatrix} \bar{m}_1 \\ \bar{v}_1 \end{bmatrix} = \begin{bmatrix} A_{10} & B_{10} \\ C_{10} & D_{10} \end{bmatrix} \begin{bmatrix} \bar{p}_0 \\ \bar{e}_0 + \overline{\Delta v} \end{bmatrix} \tag{2-11}$$

$$\begin{bmatrix} \bar{m}_2 \\ \bar{v}_2 \end{bmatrix} = \begin{bmatrix} A_{20} & B_{20} \\ C_{20} & D_{20} \end{bmatrix} \begin{bmatrix} \bar{p}_0 \\ \bar{e}_0 + \overline{\Delta v} \end{bmatrix}. \tag{2-12}$$

The cost function for this controller (Delta-Velocity Controller I) is then

$$J(\overline{\Delta v}) = \overline{\Delta v}^T Q \, \overline{\Delta v} + \bar{m}_1^T R \, \bar{m}_1 + \bar{v}_1^T R_v \, \bar{v}_1 + \bar{m}_2^T S \, \bar{m}_2 + \bar{v}_2^T S_v \, \bar{v}_2, \tag{2-13}$$

where the added weighting matrices, R_v and S_v, are positive semidefinite. (This formulation is further complicated by the addition of two weighting matrices that must be somehow chosen. In general, there does not appear to be an strategy that can optimally select the weighting matrix entries for this controller or for the station-keeping routines of Dwivedi or Howell and Pernicka. Extensive experimentation in addition to investigator judgement are often successfully used; however, a selection method for the weighting matrix entries will be a valuable area of future research.)

Using equations (2-11) and (2-12), the following equations for the residuals at time t_1 and t_2 can be found:

$$\bar{m}_1 = B_{10}\bar{e}_0 + B_{10}\overline{\Delta v} + A_{10}\bar{p}_0, \tag{2-14}$$

$$\bar{m}_2 = B_{20}\bar{e}_0 + B_{20}\overline{\Delta v} + A_{20}\bar{p}_0, \tag{2-15}$$

$$\bar{v}_1 = D_{10}\bar{e}_0 + D_{10}\overline{\Delta v} + C_{10}\bar{p}_0, \tag{2-16}$$

$$\bar{v}_2 = D_{20}\bar{e}_0 + D_{20}\overline{\Delta v} + C_{20}\bar{p}_0. \tag{2-17}$$

Recall that t_1 and t_2 are computed by adding incremental times Δt_1 and Δt_2, respectively, to the initial time t_0. Figure 2-4 is a depiction of the Delta-Velocity Controller I that uses a control input at the initial time t_0 and includes two target times (t_1 and t_2). The weighting of velocity errors in the cost function will obviously complicate the derivation.

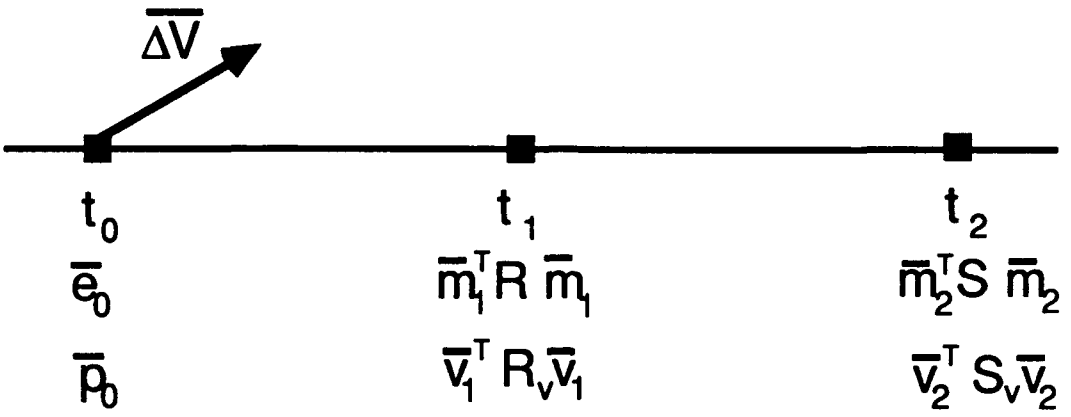

$\overline{e}_0$= VELOCITY DEVIATION FROM THE NOMINAL PATH AT TIME t_0. THIS IS A 3 x 1 VECTOR.

$\overline{p}_0$= POSITION DEVIATION FROM THE NOMINAL PATH AT TIME t_0. THIS IS A 3 x 1 VECTOR.

$\overline{m}_1$ = POSITION DEVIATION FROM THE NOMINAL PATH AT TIME t_1 IF $\overline{\Delta v}$ IS INPUT AT TIME t_0. THIS IS A 3 x 1 VECTOR.

$\overline{v}_1$ = VELOCITY DEVIATION FROM THE NOMINAL PATH AT TIME t_1 IF $\overline{\Delta v}$ IS INPUT AT TIME t_0. THIS IS A 3 x 1 VECTOR.

$\overline{m}_2$= POSITION DEVIATION FROM THE NOMINAL PATH AT TIME t_2 IF $\overline{\Delta v}$ IS INPUT AT TIME t_0. THIS IS A 3 x 1 VECTOR.

$\overline{v}_2$ = VELOCITY DEVIATION FROM THE NOMINAL PATH AT TIME t_2 IF $\overline{\Delta v}$ IS INPUT AT TIME t_0. THIS IS A 3 x 1 VECTOR.

R, S, R_v, S_v ARE 3 x 3 POSITIVE SEMIDEFINITE WEIGHTING MATRICES USED IN THE COST FUNCTION

Figure 2-4. Delta-Velocity Controller I.

Equations (2-14) through (2-17) can be substituted into equation (2-13), and the relative minimum of this function of $\overline{\Delta v}$ (after considerable algebra) is found to be

$$\overline{\Delta v}^{*} = - [\, Q + B_{10}^{T} R\, B_{10} + B_{20}^{T} S\, B_{20} + D_{10}^{T} R_{v} D_{10} + D_{20}^{T} S_{v} D_{20}\,]^{-1} \times$$

$$[(B_{10}^{T} R\, B_{10} + B_{20}^{T} S\, B_{20} + D_{10}^{T} R_{v} D_{10} + D_{20} S_{v} D_{20}^{T})\, \bar{e}_{0} +$$

$$(B_{10}^{T} R\, A_{10} + B_{20}^{T} S\, A_{20} + D_{10}^{T} R_{v} C_{10} + D_{20}^{T} S_{v} C_{20})\, \bar{p}_{0}]. \quad (2\text{-}18)$$

In the final section of the chapter, this control law will be shown to provide excellent results for station-keeping of a libration point orbit. However, when the minimum separation time between control inputs is increased to 60 or 80 days, this controller tends to exhibit an increase in cost. Perhaps a controller that looks further downtrack may provide some improvement in control costs.

D. Delta-Velocity Controller II

One way to add cost function weighting to residuals farther along the track would be to increase the size of incremental times Δt_1 and Δt_2. Alternatively, a third target point can be added to the formulation of Delta-Velocity Controller I; this adjustment can permit the target times to be approximately equally spaced (an arbitrary choice) with Δt_1 = 40 days, for instance. This adjustment will be shown to increase the robustness and decrease the cost of the station-keeping algorithm, especially when the minimum control input separation times are extended to 60 or 80 days.

For this formulation, position and velocity residuals at time t_3 are added as 3x1 vectors $\bar{m}_3$ and $\bar{v}_3$ to give:

$$\begin{bmatrix} \bar{m}_1 \\ \bar{v}_1 \end{bmatrix} = \begin{bmatrix} A_{10} & B_{10} \\ C_{10} & D_{10} \end{bmatrix} \begin{bmatrix} \bar{p}_0 \\ \bar{e}_0 + \overline{\Delta v} \end{bmatrix}, \tag{2-19}$$

$$\begin{bmatrix} \bar{m}_2 \\ \bar{v}_2 \end{bmatrix} = \begin{bmatrix} A_{20} & B_{20} \\ C_{20} & D_{20} \end{bmatrix} \begin{bmatrix} \bar{p}_0 \\ \bar{e}_0 + \overline{\Delta v} \end{bmatrix}, \tag{2-20}$$

$$\begin{bmatrix} \bar{m}_3 \\ \bar{v}_3 \end{bmatrix} = \begin{bmatrix} A_{30} & B_{30} \\ C_{30} & D_{30} \end{bmatrix} \begin{bmatrix} \bar{p}_0 \\ \bar{e}_0 + \overline{\Delta v} \end{bmatrix}. \tag{2-21}$$

Figure 2-5 depicts the elements of Delta-Velocity Controller II that includes the weighting of velocity errors at the target points, the use of three target times, and a control input at time t_0.

The cost function now includes terms for the third time step and becomes

$$J(\overline{\Delta v}) = \overline{\Delta v}^T Q\ \overline{\Delta v} + \bar{m}_1^T R\ \bar{m}_1 + \bar{v}_1^T R_v \bar{v}_1 + \bar{m}_2^T S\ \bar{m}_2 + \bar{v}_2^T S_v \bar{v}_2 + \bar{m}_3^T T\ \bar{m}_3 + \bar{v}_3^T T_v \bar{v}_3, \tag{2-22}$$

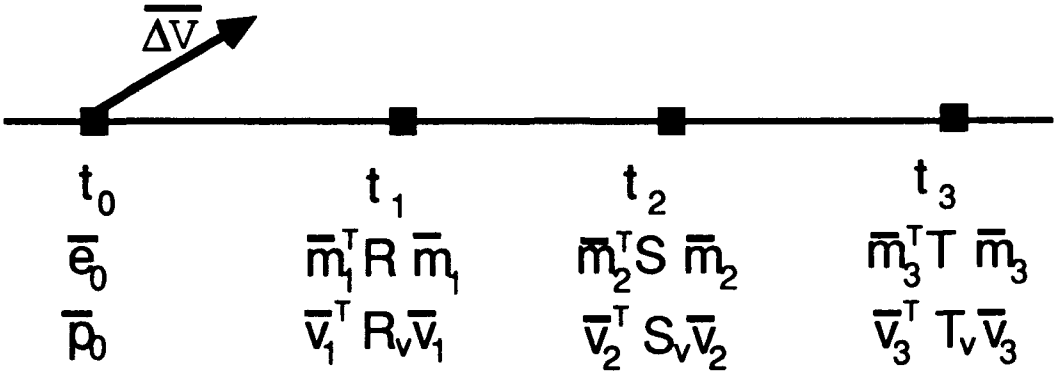

$\overline{e}_0$ = VELOCITY DEVIATION FROM THE NOMINAL PATH AT TIME t_0. THIS IS A 3 x 1 VECTOR.

$\overline{p}_0$ = POSITION DEVIATION FROM THE NOMINAL PATH AT TIME t_0. THIS IS A 3 x 1 VECTOR.

$\overline{m}_1$ = POSITION DEVIATION FROM THE NOMINAL PATH AT TIME t_1 IF $\overline{\Delta v}$ IS INPUT AT TIME t_0. THIS IS A 3 x 1 VECTOR.

$\overline{v}_1$ = VELOCITY DEVIATION FROM THE NOMINAL PATH AT TIME t_1 IF $\overline{\Delta v}$ IS INPUT AT TIME t_0. THIS IS A 3 x 1 VECTOR.

$\overline{m}_2$ = POSITION DEVIATION FROM THE NOMINAL PATH AT TIME t_2 IF $\overline{\Delta v}$ IS INPUT AT TIME t_0. THIS IS A 3 x 1 VECTOR.

$\overline{v}_2$ = VELOCITY DEVIATION FROM THE NOMINAL PATH AT TIME t_2 IF $\overline{\Delta v}$ IS INPUT AT TIME t_0. THIS IS A 3 x 1 VECTOR.

$\overline{m}_3$ = POSITION DEVIATION FROM THE NOMINAL PATH AT TIME t_3 IF $\overline{\Delta v}$ IS INPUT AT TIME t_0. THIS IS A 3 x 1 VECTOR.

$\overline{v}_3$ = VELOCITY DEVIATION FROM THE NOMINAL PATH AT TIME t_3 IF $\overline{\Delta v}$ IS INPUT AT TIME t_0. THIS IS A 3 x 1 VECTOR.

R, R_V, S, S_V, T, T_V ARE 3 x 3 POSITIVE SEMI-DEFINITE COST FUNCTION WEIGHTING MATRICES

Figure 2-5. Delta-Velocity Controller II.

where the added weighting matrices, T and T_v, are positive semidefinite. The cost function can be written in terms of $\overline{\Delta v}$ by using substitutions for $\bar{m}_k$ and $\bar{v}_k$, with k = 1, 2, and 3, derived from equations (2-19), (2-20), and (2-21). The relative minimum of this function of $\overline{\Delta v}$ (after considerable algebra) is found to be

$$\overline{\Delta v}^{*}=-[Q+B_{10}^{T}R\ B_{10}+B_{20}^{T}S\ B_{20}+B_{30}^{T}T\ B_{30}+D_{10}^{T}R_{v}D_{10}+D_{20}^{T}S_{v}D_{20}+D_{30}^{T}T_{v}D_{30}]^{-1}\times$$

$$[(B_{10}^{T}R\ B_{10}+B_{20}^{T}S\ B_{20}+B_{30}^{T}T\ B_{30}+D_{10}^{T}R_{v}D_{10}+D_{20}^{T}S_{v}D_{20}+D_{30}^{T}T_{v}D_{30})\bar{e}_{0}+$$

$$(B_{10}^{T}R\ A_{10}+B_{20}^{T}S\ A_{20}+B_{30}^{T}T\ A_{30}+D_{10}^{T}R_{v}C_{10}+D_{20}^{T}S_{v}C_{20}+D_{30}^{T}T_{v}C_{30})\bar{p}_{0}]. \qquad (2\text{-}23)$$

The general method described above could certainly accommodate the inclusion of additional target points. The relative value of using additional target points and an algorithm for selecting the weighting matrix entries both seem to be potential areas for future research. Preliminary work using entries from the state transition matrices has shown some degree of promise in choosing the weighting matrix entries. Results to date are inconclusive.

The third type of controller investigated is termed an on/off station-keeping method because the control energy is input as an acceleration, added for a few days and then removed for varying periods up to 80 days. The on/off type of controller is fundamentally a modification of a discrete-time continuous controller that is modified to be more operationally feasible.

E. On/Off Controller

The station-keeping method considered for use here is state feedback control computed from minimization of a quadratic cost function.[28-31] Other researchers[32,33] have used a similar control scheme for work concerning planned libration point orbits in the Earth-Moon and Sun-Earth systems. The method has been shown to produce competitively low control costs; however, this type of scheme has significant drawbacks for actual implementation. The method as used here assumes piecewise constant control inputs, yet thrusters typically are not designed for constant operation. (This type of thruster is being developed now, however, for use in the next decade.) Generally, impulsive control inputs are preferred in practice.

The control strategy considered here incorporates the use of a torus about the reference trajectory; the control input is delayed until the limits of the predetermined torus are violated. Because of actual mission constraints, this formulation also includes a specified minimum number of days between manuevers and a minimum control input magnitude. Simplifying assumptions, related to accommodation of the time-varying nature of the residuals, will be discussed later. All of these minimal constraints and as yet unspecified simplifying assumptions make this formulation truly "suboptimal" yet computationally simple; however, a great deal of problem insight can be gained from this analysis.

Throughout the formulation of all of the station-keeping algorithms, the reference trajectory is defined by six cubic splines, one for each of the six states. The continuous, linearized residual model is given in the following form:

$$\dot{\tilde{x}}(t) = A(t)\,\tilde{x}(t) + B\,\bar{u}(t) \tag{2-24}$$

$$\bar{u}(t) = G(t)\,\tilde{x}(t), \tag{2-25}$$

where

$$B = \begin{bmatrix} 0 & 0 & 0 \\ 0 & 0 & 0 \\ 0 & 0 & 0 \\ 1 & 0 & 0 \\ 0 & 1 & 0 \\ 0 & 0 & 1 \end{bmatrix} \tag{2-26}$$

and A(t) is the 6x6 Jacobian matrix derived in Chapter 1. The state feedback gain matrix is G(t). For computation of the piecewise constant suboptimal gains, the system (2-24) is discretized to produce:[29-31,34]

$$\tilde{x}_{k+1} = \Phi(k+1,k)\ \tilde{x}_k + B_D\ \bar{u}(k), \tag{2-27}$$

where $\tilde{x}_k$ is the residual state vector at time step k; $\Phi(k+1,k)$ is the state transition matrix at time step k+1 relative to time step k; B_D is the discrete matrix derived from B; and $\bar{u}(k) = G_k\ \tilde{x}_k$ is the piecewise constant state feedback control. The control energy is computed in an optimal way through minimization of a quadratic cost function.

The feedback gain, G_k, can be calculated by minimizing the following total cost function:

$$V(\rho) = \sum_{k=0}^{n-1} [\tilde{x}_k^T\ \rho\ Q\ \tilde{x}_k + \bar{u}^T(k)\ R\ \bar{u}(k)], \tag{2-28}$$

where Q is the diagonal weighting matrix for state residuals; R is the diagonal weighting matrix for control input; n is the number of time steps used for the control inputs; ρ is the scalar that can be used to vary "tightness"; and terminal state constraints are omitted.

The number of time steps needed for a given trajectory is determined by the time in days between each computed change in control effort and by the duration of the orbit. For example, a 6-year trajectory with control inputs computed in 20-day segments would require n = 108 control time steps. In general, minimization of the cost function $V(\rho)$ is obtained through a sequence of difference equations that can be solved by a backward sweep method.[30,31]

One further computational simplification employed here is to use the stabilizing steady-state gain solution to the cost function $V(\rho)$. This steady-state assumption ($n\to\infty$) yields the following matrix solution for the state feedback gain matrix G_k:[29]

$$G_k = -(R + B_D^T K_k B_D)^{-1} B_D^T K_k \Phi(k+1,k), \tag{2-29}$$

where

$$K_k = \Phi^T(k+1,k) K_k \Phi(k+1,k) -$$

$$\Phi^T(k+1,k) K_k B_D (R + B_D^T K_k B_D)^{-1} B_D^T K_k \Phi(k+1,k) + \rho Q, \tag{2-30}$$

$$\bar{u}_k = G_k \tilde{x}_k = [u_1, u_2, u_3]^T. \tag{2-31}$$

Equation (2-30) is the algebraic matrix "Riccati" equation used to compute optimal steady-state feedback gains. This algebraic matrix "Riccati" equation is a simplification of a matrix difference equation that has a continuous counterpart--the "Riccati" matrix differential equation used to compute optimal state feedback in continuous time-varying systems. These matrix "Riccati" equations were so named by Rudolf E. Kalman in 1960.[35] In 1724, Jacopo Francesco, Count Riccati (1676-1754) of Venice, had considered the solution of a special form of a scalar differential equation in his work in acoustics.[36,37] His equations appeared in many applications related to Bessel functions. Some 20 years earlier, James Bernoulli (1654-1705) worked on solutions to a similar differential equation.[37] Jean Le Rond D'Alembert (1717-1783) was the first to work on a more general form of these scalar differential equations and used the name "Riccati equation" for the equations of that general form.[36]

In this work, the continuous controller uses piecewise constant gains. These steady-state gains are computed for time steps of 20 days in a suboptimal scheme.[34,38] The exact equations of motion are integrated, incorporating the control inputs, in the elliptic restricted three-body model using a Runge-Kutta fifth-order numerical integration routine.

The differential equations to be integrated are then

$$\ddot{x} - 2\,\dot{\theta}\,\dot{y} = U_x + \ddot{\theta}\,y + u_1, \tag{2-32}$$

$$\ddot{y} + 2\,\dot{\theta}\,\dot{x} = U_y - \ddot{\theta}\,x + u_2, \tag{2-33}$$

$$\ddot{z} = U_z + u_3. \tag{2-34}$$

The control energy is input through the constant accelerations denoted in equations (2-32), (2-33), and (2-34) as u_1, u_2, and u_3, respectively. This state feedback controller, using steady-state gains, could be formulated to compute a new control $\bar{u}_k$ every control time step. The control time step might be every 20, 30, 45, or even 60 days. In this way, a low level of accelerative control energy, changing periodically, could be used continuously to maintain the spacecraft within a torus about the nominal path. Figure 2-6 depicts the control scheme for the discrete-time continuous controller. This type of continuous controller formulation has shown excellent results; however, the very low level of commanded control input is not operationally feasible.

A more practical station-keeping algorithm could use an on/off control scheme that would also incorporate the various minimal control constraints mentioned previously. Even though an impulsive (delta-velocity) controller is generally considered to be the currently preferred method for station-keeping, investigation of an on/off controller can lead to valuable problem insight and may someday prove useful, given future technological advances.

For the On/Off Controller, the control inputs are set at a constant magnitude for a given 20-day time period and are then off (zero magnitude) until certain minimal constrants are met or exceeded. In this formulation, the control energy is zero unless a specified acceptable deviation distance from the nominal path is violated, a minimum control separation time is exceeded, and a minimum control magnitude is surpassed. The On-Off Controller is depicted in Figure 2-7. The control effort is computed by using the spacecraft's position and velocity errors relative to the nominal state at time t_k to calculate $\bar{u}_k = G_k \tilde{x}_k$ where G_k is the constant state feedback gain matrix computed in equation (2-29) for the given control time step, and $\tilde{x}_k$ is the state vector of residuals from the nominal path.

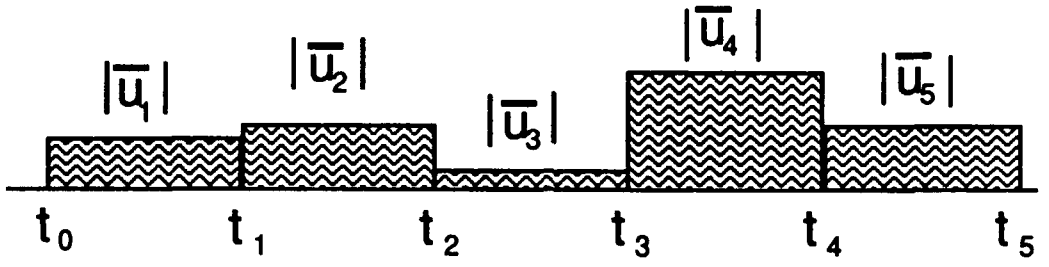

$$\overline{u_i} = [\, u_1, u_2, u_3 \,]_i \,, \; i = 1, 2, 3, \ldots\ldots$$

$$|\overline{u_i}| = [\, u_1^2 + u_2^2 + u_3^2]_i^{1/2}$$

$$t_1 - t_0 = t_2 - t_1 = t_3 - t_2 = t_4 - t_3 = t_5 - t_4 = \Delta t$$

Δt COULD BE 20 DAYS OR 30 DAYS OR 40 DAYS.....

FOR THIS RESEARCH, Δt IS 20 DAYS.

Figure 2-6. Discrete Time Continuous Controller.

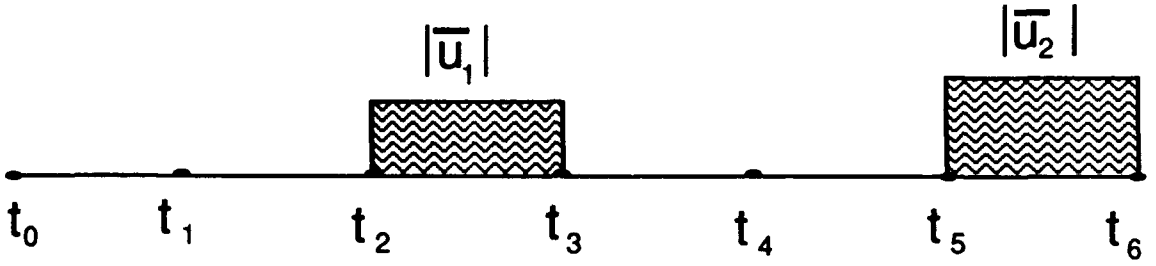

$$\overline{u_i} = [\, u_1 , u_2 , u_3 \,]_i^T , \; i = 1, 2, 3, ...$$

$$\left|\overline{u_i}\right| = [\, u_1^2 + u_2^2 + u_3^2 \,]_i^{1/2}$$

$$t_1 - t_0 = t_2 - t_1 = t_3 - t_2 = t_4 - t_3 = t_5 - t_4 = t_6 - t_5 = \Delta t$$

Δt COULD BE 20 DAYS OR 30 DAYS OR 40 DAYS.....

FOR THIS RESEARCH, Δt IS 20 DAYS.

Figure 2-7. On/Off Controller.

The weighting factors (ρ, Q, and R) in equation (2-28) determine the contribution to the total cost of deviations from the nominal path as compared to the costs of the control inputs required to counter these deviations. The positive scalar weight, ρ, has been used in other research[29,31,33] and, for this effort, ρ determines the "tightness" of the control; that is, a relatively large value of ρ causes residuals relative to the nominal path to be more costly. This will, in general, force the control algorithm to input comparatively larger control effort to maintain the spacecraft closer to the nominal path. The R weighting matrix in the cost function, $V(\rho)$, in (2-28) is arbitrarily chosen as the 3x3 identity matrix. This value for R gives the control input in each direction equal weighting.

The elements in the 6x6 diagonal matrix Q may be chosen in several ways. One particular method for choosing these entries provided results that were inconclusive here yet may prove valuable in future research. For each control time step (20 days), the entries in the Q weighting matrix were computed in a predetermined way from elements of the state transition matrix evaluated at that time step. Use of the sensitivities reflected in the state transition matrix slightly decreased the total control cost corresponding to this station-keeping method. This selection method for the elements of the Q weighting matrix is an area for future investigation and is not presented here.

Secondly, both the continuous and the on/off control methods can incorporate the estimated off-course deviation from the nominal path at the end of a control time step in order to modify the control effort input at the start of the step. This "shooting method" uses the otherwise planned control input to predict the resulting error at the end of the control time step or at some point further along the track, and then adjusts the initial gains to accommodate the predicted errors. This modification has been shown to substantially decrease the total control costs as compared to other adjustments investigated in this research. The results of several differing station-keeping methods are now presented in Chapter 3.

CHAPTER 3: STATION-KEEPING RESULTS AND COMPARISONS

Ideally, the control scheme modifications that are investigated here and the overall results from this preliminary work should be compared to other Lagrange point station-keeping results. A criteria for this comparison could be the magnitude of the total control effort that is needed to successfully maintain the vehicle, satisfying all station-keeping requirements, for a libration point orbit of some fixed duration. The fixed duration for these comparisons will be a 2-year segment of the nominal trajectory. The results of the various station-keeping approaches that are evaluated in this research will be shown to produce excellent results. However, before presenting any results and then discussing the comparisons, it is necessary to address two additional questions:

1. Are the Δv random variables (approximately) normally distributed?
2. What is a reasonable sample size?

In this section, the results of each 2-year station-keeping simulation is considered a function of several random inputs and is, therefore, treated as a random trial. Each station-keeping simulation produces a total propellant value (Δv_T) that is a scalar measure of the cost of station-keeping for that 2-year period. The simulation that produces the Δv_T variable is subject to several random inputs and, consequently, will vary for each Monte Carlo trial (simulation) of the station-keeping algoritm. Several independent simulations (random trials), where the input random variables have consistent statistical characteristics (mean and variance), will produce a random sample of Δv_T results (one for each simulation). That is, each station-keeping

run is treated as a random trial with random variable Δv_T (the magnitude of total $\overline{\Delta v}$ for the two-year orbit), and a group of random trials for which all the input variables (torus size, tracking error levels, etc) remain the same are then treated as a random sample. This resulting sample can then be tested to see if it fits the Gaussian distribution; the somewhat related question of the required number of station-keeping runs per sample must then be addressed.

If the results of the station-keeping simulations were simply a linear combination of Gaussian random variables, the resulting distribution of Δv_T would be Gaussian. This simple representation is not true here; therefore, it is necessary to complete a chi-squared goodness of fit test on the results of several trial runs in an initial sample. (Certainly, there are other statistical tests that can be used to determine whether a sample is drawn from a Gaussian distribution; the chi-squared test is not the most powerful, but it is the most easily presented.) Choosing a sufficiently large sample size, comparing population means, and constructing confidence intervals can be simplified by knowing the probability distribution of the propellant costs. Hence, the computation of a sufficient sample size apriori will permit the comparison of station-keeping methods with a minimal number of simulation runs.

The results and comparisons that follow also include statistical comparison tests for equivalent variances and equivalent means of the values for Δv_T resulting from station-keeping analyses using Lissajous and halo-type nominal orbits. The test for equivalent means between populations of, say, halo-type and Lissajous orbit propellant costs (Δv_T) requires the use of a pooled variance equation.[39] The pooled variance equation in turn assumes that the sample variances are from populations with equivalent variances; therefore, the statistical hypothesis test for equal population variances will logically preceed the test for equal population means.

A. Distribution of Delta-Velocities

Histograms of Monte Carlo simulations for the Delta-Velocity Controller II and the On/Off Controller are shown in Figures 3-1 and 3-2, respectively. The histograms are plotted using ten classes of equal width. The vertical axis is the relative frequency of the values of Δv_T in that class. The propellant costs (values of Δv_T) for station-keeping on a 2-year halo-type orbit are plotted along the horizontal axis. The class midpoints are labeled; however, the relative magnitudes of the Δv_T results for these two controllers should not be used to compare the two controllers. This comparison of Δv_T values for the various station-keeping algorithms will be completed later in this section. Both histograms show a close resemblance to a histogram based on the Gaussian distribution. (Recall that the general shape of a Gaussian distribution is determined by the variance; the sample mean affects the expected frequencies computed from the Gaussian probability distribution and thus also helps to determine the shape of the histogram that could be constructed using expected frequencies.) In Figures 3-1 and 3-2, the observed frequencies from the sample are printed above the classes in the histograms. The approximate expected frequencies, computed from the Gaussian distribution using the means and standard deviations of the samples, are printed in parentheses below the classes of the histograms.

The chi-squared goodness of fit test is appropriately used here to verify mathematically that the frequency distribution used to construct the given histogram fits the Gaussian distribution. In order to investigate this resemblance, the hypotheses tested and the decision rule are:

Hypotheses:

H_0: Distribution is Normal.

H_1: Distribution is not Normal.

Decision Rule:

If $X^2 \leq \chi^2$, conclude H_0.

Otherwise, conclude H_1.

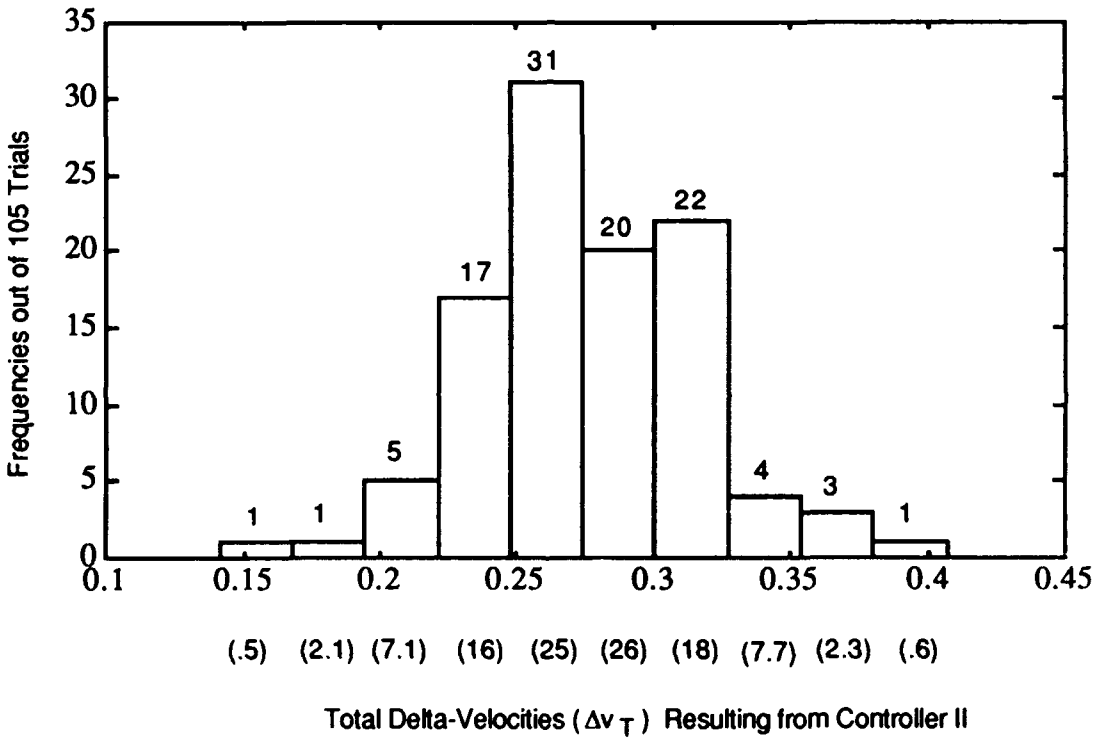

Figure 3-1. Histogram for Total Delta-Velocities Resulting from use of Controller II.

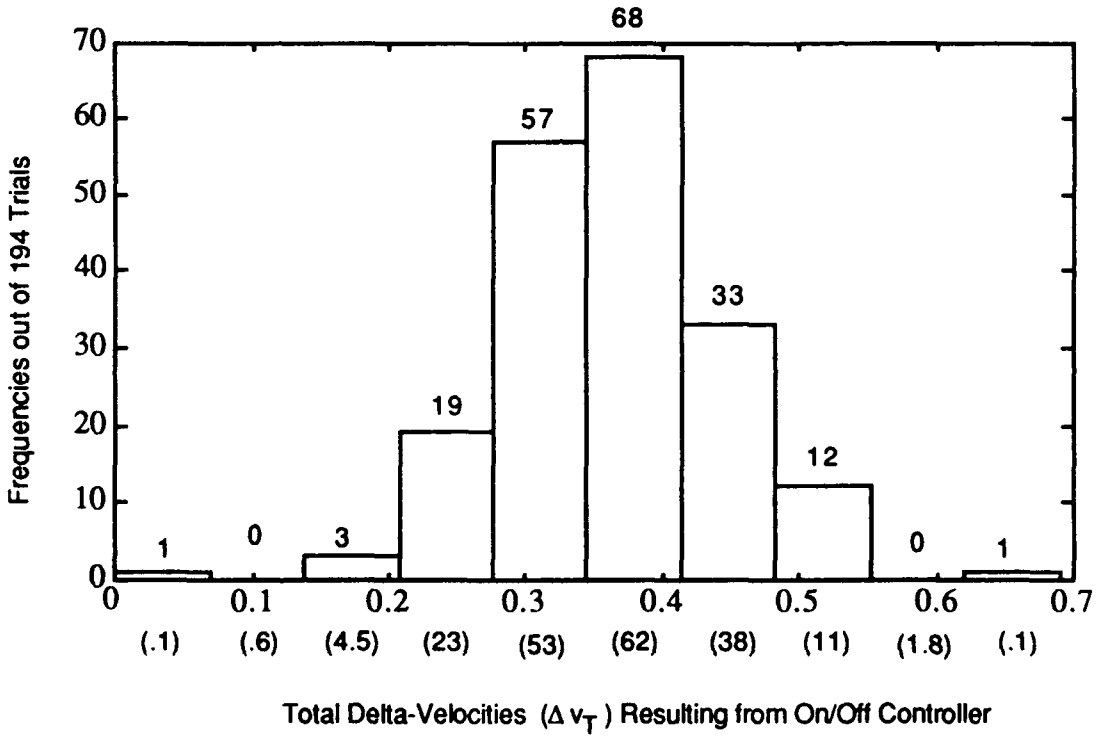

Figure 3-2. Histogram of Total Delta-Velocities Resulting from use of the On/Off Controller.

Typically, the chi-squared goodness of fit test includes the listing of expected frequencies (F_i) that are computed under the assumption that the null hypothesis (H_0) is true. The null hypothesis here is that the distribution of the values of Δv_T follows the Gaussian distribution; therefore, the ten class boundaries must be determined in terms of the standardized normal variable (Z) in preparation for computation of the expected class probabilities. The class boundaries in terms of the standardized normal variable can then be used with a standard table of probability values for the Gaussian distribution to compute expected probabilities. The expected frequencies for each class can then be calculated. The expected frequencies (F_i) and the observed frequencies (the f_i that can be read directly from the histograms or frequency distributions) are then used in the computation of the test statistic. The test statistic X^2 can be calculated as

$$X^2 = \sum_{i=1}^{k} \frac{(f_i - F_i)^2}{F_i}. \qquad (3\text{-}1)$$

Table 3 summarizes the mathematics of the chi-squared goodness of fit test for the frequency distribution of the Delta-Velocity Controller II in Figure 3-1.

For this test, the chi-squared random variable (χ^2) has k-2-1 = 5 degrees of freedom, reduced due to required pooling. (Pooling is required because the expected frequency in any class must be at least two for the chi-squared goodness of fit test.) The level of confidence is 95%. Therefore, $\chi^2 = 11.07$. For the distribution depicted by the histogram in Figure 3-1,

$$X^2 = \sum_{i=1}^{k} \frac{(f_i - F_i)^2}{F_i} = 6.639.$$

Table 3. Chi-Squared Goodness of Fit Test for Figure 3-1.

Class Boundaries		Z Values		Probability	F_i	f_i	X_i^2
.1415	.1681	$-\infty$	-2.622	.0044	.462 }*	1 }*	.1233
.1645	.1946	-2.622	-1.973	.0200	2.100	1	
.1946	.2211	-1.973	-1.325	.0674	7.077	5	.6096
.2211	.2477	-1.325	- .676	.1565	16.433	17	.0196
.2477	.2742	- .676	- .027	.2397	25.169	31	1.3512
.2742	.3007	- .027	.621	.2440	25.620	20	1.2328
.3007	.3273	.621	1.278	.1673	17.567	22	1.1190
.3273	.3538	1.278	1.919	.0729	7.655	4	1.7447
.3538	.3803	1.919	2.567	.0222	2.331 }*	3 }*	.4384
.3803	.4068	2.567	∞	.0052	.546	1	
							X^2=6.639

(Note: The symbol * indicates pooling.)

The other frequency distribution whose histogram is displayed in Figure 3-2 yields a similar small value for X^2. The decision rule then leads to the conclusion that the distribution of the Δv_T values is normal for both controllers. For normally distributed random variables, small sample sizes (less than 30) can be used, and there can still be confidence that the sample means are normally distributed. Unless the distribution of the Δv_T values was highly skewed, a sample size of 30 would generally ensure that the sample means were approximately normally distributed. Therefore, confidence intervals, using the standard normal (Z) or student's (t) distribution can be readily constructed using sample sizes of 30.

One other restriction on the minimum sample size could be the required width of the confidence intervals. Specifically, the larger the random sample size, the narrower the resulting confidence interval for the mean. The need for a "narrow" confidence interval must therefore be weighed against the difficulty in gathering the data. A

sample, as used here, is a group of station-keeping (Monte Carlo) simulations for which the minimal constraints are the same and the input errors have identical means and variances. A sample can then also be termed a "case" for later comparison with other cases (samples). The sample size is denoted here by the symbol "n", and sample sizes of 30 are generally adequate to ensure that the sample means are at least approximately normally distributed. However, this value of n must also be large enough to make "useful" confidence intervals.

B. Sample Sizes for Simulation Runs

One goal that motivates the use of several random trials (simulations) of a station-keeping algorithm is the desire to construct confidence intervals for the mean Δv_T, here denoted as $\hat{\Delta v}$ for the sample. A sample size of perhaps 20 (or even 40) for a normally distributed random variable may not provide a confidence interval that is narrow enough for comparison purposes. Too many runs can, alternatively, be inefficient while adding little to the value of the study. The selection of an appropriate sample size requires the choice of confidence level (derived from the selected α risk) and interval half width (h). The standard deviation of the population is the parameter σ that can be estimated by the sample statistic s (sample standard deviation). The confidence interval for the actual population mean μ is typically constructed surrounding the sample mean ($\hat{\Delta v}$), such that:

$$\hat{\Delta v} + (-Z\ \sigma)/n^{1/2} \leq \mu \leq \hat{\Delta v} + (Z\ \sigma)/n^{1/2}, \qquad (3\text{-}2)$$

or

$$\hat{\Delta v} \quad -h \quad \leq \mu \leq \hat{\Delta v} + \quad h. \qquad (3\text{-}3)$$

Therefore,

$$h = (Z\ \sigma)/n^{1/2}. \tag{3-4}$$

Solving for n results in the following approximate guideline for selecting a sample size:

$$n = (Z\ \sigma)^2/h^2 \cong (Z\ s)^2/h^2. \tag{3-5}$$

Notice that this estimate for n uses an approximate value (s) for σ and a judgement concerning the size of an acceptable half width (h). The Z value is obtained from tables that are available for the standardized normal variable, using the fact that one-half of the α risk is placed in each tail of the distribution. By choosing h to be less than approximately 10% of a $\hat{\Delta v}$ value that is equal to .2753, h can be selected as .020 meters per second. The sample standard deviation (s) is .0409 meters per second. The standard normal variable, computed for α = .01 (a level of confidence of 99%), is 2.576. Hence,

$$n = [(2.576)(.0409)]^2/(.020)^2 = 27.75 \rightarrow 28 \text{ (round up)}.$$

Clearly, this is a very approximate method to select the sample size n; however, sample sizes of 30 should clearly provide sufficiently accurate confidence intervals. The value of the half width (h) for a given confidence interval will depend on the sample's standard deviation (s). In other samples, it will undoubtedly differ from the .020 meters per second used in this example. However, knowing that the Δv_T random variables are approximately normally distributed and, in one case, a very narrow confidence interval could be constructed with a sample size of 28, further Monte Carlo simulations are completed using 30 runs for each sample.

C. Results and Comparisons

In this section, results from station-keeping simulations are presented. Each station-keeping method discussed earlier is represented. The results are listed in the order in which the algorithms were derived, and the population variances and values of the mean Δv_T (denoted as $\hat{\Delta v}$) are statistically compared for station-keeping relative to the halo-type or Lissajous orbit defined earlier. The final subsection provides a survey of libration point orbit station-keeping costs listed in some other works. Note that the following notation will be employed in this section for convenience: Δt_{min} is the minimum time between control inputs, Δv_{min} is the minimum control input magnitude, d_{min} is the minimal distance of the spacecraft from the nominal path before a control input is allowed (this is then also the size of the acceptable torus); $\Delta \bar{v}$ is an individual (vector) delta-velocity input with magnitude Δv; Δv_T is the (scalar) total delta-velocity resulting from a single 2-year station-keeping simulation; "n" is the number of simulations in a given sample and is often called the sample size; $\hat{\Delta v}$ is the (scalar) average of all the Δv_T values in a given sample of n simulations; "*s*" is the standard deviation from the sample of n simulations; and a "case" is a sample of n station-keeping simulations for which the means and variances of all the input variables plus the constraints are held at consistent levels.

1. Delta-Velocity Controller I Results

The first delta velocity controller derived in this work provides excellent station-keeping costs when the minimum time that must elapse between manuevers (Δt_{min}) is specified as 40 or 60 days. The results when Δt_{min} is equal to 80 days are less promising; however, these costs may be substantially reduced by an improved selection method for the target times (described below) and weighting matrix entries. Both subjects would certainly be areas for future research effort.

The target times are chosen for this work depending on the value of Δt_{min} (which is certainly not the only method of choosing the targets) and are summarized as one of three possibilities:

Δt_{min} = 40 days then $t_1 = t_0 + 20$ days and $t_2 = t_0 + 40$ days,

Δt_{min} = 60 days then $t_1 = t_0 + 40$ days and $t_2 = t_0 + 60$ days,

Δt_{min} = 80 days then $t_1 = t_0 + 40$ days and $t_2 = t_0 + 80$ days.

The weighting matrix entries are held constant for these comparisons (other methods of weighting matrix computation could also have been used):

$$R = 100 \begin{bmatrix} 1 & & \\ & 1 & \\ & & 1 \end{bmatrix},$$

$$R_v = 10 \begin{bmatrix} 1 & & \\ & 1 & \\ & & 1 \end{bmatrix},$$

$$S = S_v = \begin{bmatrix} 1 & & \\ & 1 & \\ & & 1 \end{bmatrix},$$

$$Q = 10^{-14} \begin{bmatrix} .01 & & \\ & .1 & \\ & & 1 \end{bmatrix}.$$

The results of five samples (five cases) with sample sizes of 30 each for the 2-year station-keeping simulations are depicted in Table 4. These cases for Delta-Velocity Controller I are labeled in the first column as I-1, I-2, etc. The column labeled as "Δt_{min}" indicates the minimum separation in days between control inputs for that case. The column "Δv_{min}" indicates the minimum control energy in meters per second that must be exceeded by a computed Δv before it will be implemented. These minimum Δv values agree with values used in other libration point orbit station-keeping studies.[40,41] An investigation by Longuski and Todd[42] also gives considerable insight into the magnitudes of the various force levels affecting the spacecraft. Their findings have been used to help determine the minimum control energy levels that can be used in this effort. The symbol "d_{min}" (torus size) is in kilometers and indicates the distance the spacecraft must be from the nominal path before a control force will be input. All three restrictions (Δt_{min}, Δv_{min}, and d_{min}) must be met or exceeded before a control input is possible.

The average 2-year Δv_T for the Lissajous orbit is indicated by $\hat{\Delta v}_L$; for the halo-type orbit, it is denoted $\hat{\Delta v}_h$. The sample standard deviations are s_L for the Lissajous orbit and s_h for the halo-type orbit. Sample means and standard deviations are given in meters per second. These sample means and standard deviations, as listed in Table 4, are, in general, not equal for the two different types of orbit within each case (that is, $\hat{\Delta v}_L \neq \hat{\Delta v}_h$ and $s_L \neq s_H$ within each case); however, the differences may not be statistically significant. The significance of the differences will be discussed shortly.

The results depicted in Table 4 are derived from simulations using the nominal orbits depicted in Figures 3-1 and 3-2. The nominal orbits are thought to be representative of those being considered for near-term missions. However, due to the virtually infinite variety of sizes and shapes for these types of orbits, no claim can be made that these results would apply to *all* libration point orbits.

Table 4. Sample Means and Standard Deviations for Controller I.

#	Δt_{min} (days)	Δv_{min} (m/s)	d_{min} (km)	Lissajous Orbit $\hat{\Delta v}_L$ (m/s)	Lissajous Orbit s_L (m/s)	Halo-Type Orbit $\hat{\Delta v}_H$ (m/s)	Halo-Type Orbit s_H (m/s)
I-1	40	.015	0	.3276	.0737	.3395	.0717
I-2	40	.050	100	.7994	.0903	.7845	.1099
I-3	60	.015	0	1.0602	.7597	.8945	.9088
I-4	60	.050	100	1.3909	.5180	1.2804	.3105
I-5	80	.015	0	10.4138	12.8951	13.2013	10.3289

Table 5 contains other useful data concerning the Delta-Velocity Controller I samples. This data includes the range of values for the random trials within each case. For instance, in case I-1, at least one of the random trials (one 2-year Δv_T) for a Lissajous orbit had the minimum Δv_T value of .18 meters per second. In the same sample, at least one run had the maximum Δv_T value of .49 meters per second. The range and the standard deviation are both measures of dispersion for the samples.

Table 5. Ranges for Δv_T's and Number of Δv's for Controller I.

#	Δt_{min} (days)	Δv_{min} (m/s)	Torus (km)	Lissajous Orbit $\hat{\Delta v}_L$ (m/s)	Lissajous Orbit Range (m/s)	Halo-Type Orbit $\hat{\Delta v}_H$ (m/s)	Halo-Type Orbit Range (m/s)	Average Number of Δv's
I-1	40	.015	0	.3276	.18-.49	.3395	.23-.54	14-15
I-2	40	.050	100	.7994	.65-1.00	.7845	.59-1.03	10-11
I-3	60	.015	0	1.0602	.26-2.92	.8945	.27-4.46	9-10
I-4	60	.050	100	1.3909	.62-3.02	1.2804	.74-2.01	8-9
I-5	80	.015	0	10.4138	.72-31.9	13.2013	.63-35.3	7-9

The average number of individual Δv's applies to both the Lissajous and halo-type orbits; it is the median number of control inputs required for the 2-year station-keeping simulations within a given case (sample). Notice that in case I-5, one or more of the 30 random station-keeping trials required only 7 manuevers over the 2-year period.

It is now straightforward to test whether the "type" of orbit (Lissajous or halo-type) affects the resulting 2-year station-keeping costs. The statistical test for equal means assumes approximately equal sample variances, hence that will be a natural first test to conduct. The statistical hypothesis test for equal variances assumes that the test statistic (s_H^2/s_L^2) follows Fisher's F probability distribution. The F distribution has two types of degrees of freedom (numerator and denominator) and is tabulated also in terms of the level of confidence. The degrees of freedom are 1 less than the respective sample size (which is n) for the numerator and denominator samples; so that the degrees of freedom in this example are 29 (which is n-1) for both the numerator and denominator. An F statistic denoted by $F_{(29,29,.995)}$ indicates 29 degrees of freedom for both the numerator and denominator and a level of confidence of 99%. The α risk is then .01 and is divided equally between lower and upper bounds in the decision rule. The test statistic is $F^* = (s_H^2/s_L^2)$, and the hypotheses and decision rule are:

Hypotheses:

$H_0: \sigma_H^2 = \sigma_L^2$ (Variances for halo-type and Lissajous orbits are equal.)

$H_1: \sigma_H^2 \neq \sigma_L^2$

Decision Rule:

If $F_{(29,29,.005)} \leq (s_H^2/s_L^2) \leq F_{(29,29,.995)}$, conclude H_0.

Otherwise, conclude H_1.

In the work that follows, the lower F statistic in the decision rule is labeled as F_{low}; the upper F statistic is denoted F_{up}. The F distribution value is $F_{(29,29,.995)} = F_{up} = 2.7$. The value of F_{low} is derived from the value of F_{up} and is given by $F_{(29,29,.005)} = F_{low} = 1/2.7 = .3704$.

The cases I-1 through I-5 in Table 5 can now be analyzed for equal variances. The numerical results and the hypothesis test conclusions are summarized in Table 6.

Table 6. Results of Equal Variance Tests for Controller I.

#	s_L (m/s)	s_H (m/s)	F_{low}	F^*	F_{up}	Conclusion
I-1	.0737	.0717	.3704	.9465	2.7	H_0
I-2	.0903	.1099	.3704	1.4812	2.7	H_0
I-3	.7597	.9088	.3704	1.4310	2.7	H_0
I-4	.5180	.3105	.3704	.3593	2.7	H_1
I-5	12.8951	10.3289	.3704	.6416	2.7	H_0

Thus, in four out of the five cases, the variances can be assumed to be equal. In general, there is some finite risk of finding in favor of H_1 even when H_0 is true; however, this α risk (.01) was chosen to be very low in this case. The hypothesis tests for equal population means corresponding to case I-4 should only continue if some rough equivalence of variances can be determined for it. Further samples in this case could be compiled so that the hypothesis test for case I-4 could be redone, and this could result in substantial problem insight. However, the failure by a small margin for the hypothesis test for only this case could also allow the use of a more liberal and general rule of thumb: if the sample variances are within approximately one order of magnitude, the pooled variance equation can be correctly used.

Therefore, the hypothesis test for equal population means may be pursued in all of these cases I-1 through I-5.

The statistical hypothesis test for equal population means (μ_L for Lissajous and μ_H for halo-type orbit delta-velocities) assumes that the difference between the two population means is distributed according to the Student's t distribution. The test statistic is t^* and is a function of the difference between the sample means $(\hat{\Delta v}_H - \hat{\Delta v}_L)$.

The pooled variance equation is

$$s_c^2 = \frac{(n_L-1)s_L^2 + (n_H-1)s_H^2}{(n_L-1) + (n_H-1)}, \tag{3-40}$$

where the number of random trials for both Lissajous (n_L) and halo-type (n_H) orbits is 30 in this work. The test statistic is

$$t^* = \frac{(\hat{\Delta v}_H - \hat{\Delta v}_L)}{s_c(1/n_L + 1/n_H)^{1/2}}.$$

The hypotheses and decision rule are:

Hypotheses:

$H_0: \mu_L = \mu_H$.

$H_1: \mu_L \neq \mu_H$.

Decision Rule:

If $-t \leq t^* \leq t$, conclude H_0.

Otherwise, conclude H_1.

The α risk of .01 is again equally divided in both tails of the t distribution. For this hypothesis test, the degrees of freedom are equal to $(n_L-1) + (n_H-1)$, and the t statistic is $\pm t_{(.995,58)} = \pm 2.66$.

The numerical results and the conclusions are depicted in Table 7.

Table 7. Results of Equality of Means Tests for Controller I.

#	$\hat{\Delta v}_L$ (m/s)	$\hat{\Delta v}_H$ (m/s)	-t	t^*	t	Conclusion
I-1	.3276	.3395	-2.66	.6314	2.66	H_0
I-2	.7994	.7845	-2.66	-.5736	2.66	H_0
I-3	1.0602	.8945	-2.66	-.7661	2.66	H_0
I-4	1.3909	1.2804	-2.66	n/a	2.66	n/a
I-5	10.4138	13.2013	-2.66	.9241	2.66	H_0

The hypothesis test conclusions are then, in general, that there is no significant statistical difference between the 2-year station-keeping costs for the Lissajous and halo-type orbits identified in the study when Delta-Velocity Controller I is used. The entries "n/a" in Table 7 are for the case I-4 for which the hypothesis test for equivalent variances led to the conclusion in favor of $H_1: \sigma_H^2 \neq \sigma_L^2$. If the variances were pooled, t^* for this case would be -.9853, and the conclusion would also be in favor of equal means ($H_0: \mu_L = \mu_H$).

Now that the statistical hypothesis tests for equal population variances and equal population means between halo-type and Lissajous orbits have been completed for this controller, two more short analyses seem appropriate. Station-keeping error analysis will look at the station-keeping (propellant) costs that can be attributed to each error source. Finally, confidence intervals for the mean Δv_T cost for each case can be constructed here and used later in the comparison subsection. A limited station-keeping error analysis for this station-keeping method has been conducted, and the results are shown in Table 8.

This error analysis seeks to quantify the relative contributions of the individual error sources modeled in the simulations. The data in Table 8 corresponds to results for the halo-type orbit shown in

Figure 1-5. The injection and tracking error levels are those computed in the chapter two orbit determination error analysis of this work for a halo-type orbit, and the results found here are compared to those

Table 8. Station-Keeping Error Analysis Results.

	Contribution	
Error Source	This Work	Simó[62]
Injection Errors	2.5%	n/a
Control Errors (10%)	2.0%	10.0%
Tracking Errors	55.9%	50.0%
Solar Reflectivity Uncertainty	35.0%	15.0%
Force Model and Integration	4.6%	25.0%

found in Simó.[40] The major difference between the error analysis in this work and the station-keeping error analysis in Simó is that his study uses random solar reflectivity errors with a standard deviation of 2.5% versus the 13% used here. A second difference is that this work also includes gravitational parameter uncertainty in the tracking error levels. (The nominal orbit used in Simó may also be slightly different from the halo-type orbit used here.) Because of the increased level of solar reflectivity and gravitational parameter uncertainty, the overall error level is considerably larger, and the smaller contributors (such as control errors and integration errors) provide a relatively smaller percentage of the total control costs.

Lastly, confidence intervals for the mean Δv_T used in both types of orbits can also be constructed. The form of these confidence intervals used later in this chapter are

	Lower Limit		Upper Limit
Lissajous orbit:	$\hat{\Delta v}_L + (-t\ s_L)/n_L^{1/2}$	$\leq \mu_L \leq$	$\hat{\Delta v}_L + (t\ s_L)/n_L^{1/2}$
Halo-type orbit:	$\hat{\Delta v}_H + (-t\ s_H)/n_H^{1/2}$	$\leq \mu_H \leq$	$\hat{\Delta v}_H + (t\ s_H)/n_H^{1/2}$.

The t statistic will have n_L-1 and n_H-1 degrees of freedom for the Lissajous and halo-type orbits' confidence intervals, respectively. An α risk of .01 is used to give a t statistic of 2.462. The numerical results are depicted in Table 9.

Table 9. Confidence Intervals for Controller I.

#	Lissajous Orbit (m/s)		Halo-Type Orbit (m/s)	
	Lower Limit	Upper Limit	Lower Limit	Upper Limit
I-1	.2946	.3607	.3073	.3717
I-2	.7588	.8400	.7351	.8339
I-3	.7187	1.1020	.4860	1.3030
I-4	1.1581	1.6237	1.1408	1.4200
I-5	4.6175	16.2101	8.5585	17.8440

Notice that there is considerable overlap of the intervals in each case for the halo-type and Lissajous orbits. These 99% confidence intervals can be used later to compare the station-keeping costs of Delta-Velocity Controller I with several other approaches such as Delta Velocity Controller II.

2. Delta-Velocity Controller II Results

The formulation of Delta-Velocity Controller II requires the selection of seven weighting matrices (two more than are needed for controller I). The formulation also requires the determination of three target times. The weighting matrices used for these simulations were set for all trials at:

$$R = 100 \begin{bmatrix} 1 & & \\ & 1 & \\ & & 1 \end{bmatrix},$$

$$R_v = 10 \begin{bmatrix} 1 & & \\ & 1 & \\ & & 1 \end{bmatrix},$$

$$S = S_v = \begin{bmatrix} 1 & & \\ & 1 & \\ & & 1 \end{bmatrix},$$

$$\Gamma = T_v = \begin{bmatrix} .1 & & \\ & .1 & \\ & & .1 \end{bmatrix},$$

$$Q = 10^{-14} \begin{bmatrix} .01 & & \\ & .1 & \\ & & 1 \end{bmatrix}.$$

The target times are selected such that if

Δt_{min}=60 days then $t_1=t_0+$ 25 days, $t_2=t_0+$ 50 days, and $t_3=t_0+$ 75 days,

or

Δt_{min}=80 days then $t_1=t_0+$ 30 days, $t_2=t_0+$ 60 days, and $t_3=t_0+$ 90 days.

This second delta-velocity controller has been evaluated under similar test conditions as in cases I-4 and I-5 for the first delta-velocity controller. Here, they are labeled as cases II-1 and II-2, respectively. (See Table 5 for parameter selections in cases I-4 and I-5.) Cases I-4 and II-1 differ only in the selection of weighting matrices and target times; case II-2 uses a larger Δv_{min} and larger d_{min} than case I-5. Clearly, the same hypothesis tests can be conducted on these controller II cases, and confidence intervals can also be constructed. Some of the numerical results for cases II-1 and II-2 are summarized in Table 10. The notation used here is identical to that used for Table 4.

Table 10. Sample Means and Standard Deviations for Controller II.

				Lissajous Orbit		Halo-Type Orbit	
#	Δt_{min} (days)	Δv_{min} (m/s)	d_{min} (km)	$\hat{\Delta v}_L$ (m/s)	s_L (m/s)	$\hat{\Delta v}_H$ (m/s)	s_H (m/s)
II-1	60	.050	100	.8450	.1603	.8124	.1233
II-2	80	.050	100	1.0852	.4682	1.0740	.3436

The average Δv_T for case I-4 was 1.3909 meters per second for the Lissajous orbit and 1.2804 mete per second for the halo-type orbit. The improvement in station-keeping costs is significant and perhaps indicates that future work with this controller may be quite valuable. Other numerical results for Controller II are listed in Table 11. The notation used here is identical to that used in Table 5.

Table 11. Sample Ranges and Number of Control Inputs for Controller II.

#	Δt_{min} (days)	Δv_{min} (m/s)	d_{min} (km)	Lissajous Orbit $\hat{\Delta v}_L$ (m/s)	Lissajous Orbit Range (m/s)	Halo-Type Orbit $\hat{\Delta v}_H$ (m/s)	Halo-Type Orbit Range (m/s)	Average Number of Δv's
II-1	60	.050	100	.8450	.57-1.15	.8124	.62-1.08	7-8
II-2	80	.500	100	1.0852	.49-2.40	1.0740	.63-2.03	7-8

Both cases show that some simulations incorporating this station-keeping strategy require as few as seven manuevers over the entire 2-year simulation. The range of Δv_T values for both halo-type and Lissajous orbits is again listed as another measure of the samples' dispersion. The data in Tables 10 and 11 can now be tested for equality of variance and equality of population means between halo-type and Lissajous orbits within each case.

Initially, the hypothesis that the population variances are equal is tested. The hypothesis test procedures and the notation are identical to those used for these tests when evaluating results from use of Controller I. The hypothesis test and the decision rule are summarized below; the numerical results and conclusions are listed in Table 12:

Hypotheses

$$H_0: \sigma_H^2 = \sigma_L^2$$

$$H_1: \sigma_H^2 \neq \sigma_L^2$$

Decision Rule

$$\text{If} \quad F_{(29,29,.005)} \leq (s_H^2/s_L^2) \leq F_{(29,29,.995)}, \text{ conclude } H_0.$$

Otherwise, Conclude H_1.

Therefore, with 99% confidence, it can be concluded that the population variances are equal when considering cases II-1 and II-2 (resulting from use of the Delta-Velocity Controller II). Once population variances are found to be equal, the pooled variance can be calculated and the hypothesis test for equal population means can be completed.

Table 12. Results of Tests for Equal Variances for Controller II.

#	s_L (m/s)	s_H (m/s)	F_{low}	F^*	F_{up}	Conclusion
II-1	.1603	.1233	.3704	.5916	2.7	H_0
II-2	.4682	.3436	.3704	.7339	2.7	H_0

Again, the hypothesis test for equal population means is conducted using the t distribution. The hypotheses and decision rule are

Hypotheses:

$H_0: \mu_L = \mu_H$.

$H_1: \mu_L \neq \mu_H$.

Decision Rule:

If $-t \leq t^* \leq t$, conclude H_0.

Otherwise, conclude H_1.

The α risk of .01 is again equally divided in both tails of the t distribution. The degrees of freedom are, for this hypothesis test, equal to $(n_L-1) + (n_H-1)$ and the t statistic is $\pm t_{(.995,58)} = \pm 2.66$. The numerical results and the conclusions are listed in Table 13.

For Delta-Velocity Controller II, the results clearly indicate that the means for both types of orbits for cases II-1 and II-2 are equal with a 99% level of confidence. Now, in order to prepare for later cost comparisons, confidence intervals for the mean propellant costs can be constructed.

Table 13. Test Results for Equality of Means for Controller II.

#	$\hat{\Delta v}_L$ (m/s)	$\hat{\Delta v}_H$ (m/s)	-t	t^*	t	Conclusion
II-1	.8450	.8124	-2.66	.4486	2.66	H_0
II-2	1.0852	1.0746	-2.66	.0344	2.66	H_0

The confidence intervals within both cases can be easily formulated, again using the t distribution. An α risk of .01 is used to give a t statistic of 2.462. The computed intervals for cases that include both Controllers I and II are listed in Table 14.

Table 14. Confidence Intervals for the Mean for Controller II.

#	Lissajous Orbit (m/s)		Halo-Type Orbit (m/s)	
	Lower Limit	Upper Limit	Lower Limit	Upper Limit
I-4	1.1581	1.6237	1.1408	1.4200
II-1	.7729	.9171	.7570	.8678
I-5	4.6175	16.2101	8.5585	17.8440
II-2	.8747	1.2957	.9200	1.2285

Clearly, Delta-Velocity Controller II exhibits a great improvement over Delta-Velocity Controller I for cases involving Δt_{min} = 80 days, that is, a minimum control input separation time of 80 days. The improvement may not completely be due to the added complexity of Controller II. In fact, Controller I may yield much improved costs when alternative weighting matrix entries and target times are selected. This is certainly an area for future inquiry.

3. State Feedback Controllers

The state feedback controller formulated in this work can be used as a Continuous Controller or as an On/Off Controller. The results associated with use of the On/Off Controller are primarily summarized here. The Continuous Controller was developed in early research and did not incorporate the realistic constraint of a minimum control level, nor the use of a minimum deviation distance relative to the nominal path. The station-keeping costs resulting from simulations that incorporate the Continuous Controller are quite low; however, spacecraft thrusters that can deliver continuous low thrust are not currently operational, but are in development for use in the next decade. The low level of thrust that may be required to implement the Continuous Controller may still be too low for the engines currently in development, and the computed thrust level may be of the same order of magnitude as the uncertainty levels of other forces on the spacecraft. As noted previously, in an important work concerning this topic, Longuski and Todd[42] have done extensive research in the area of quantifying the various force levels on a spacecraft in orbit in this solar system. The results of their work are used to help determine the minimal control energy that is practical for this controller.

a. Continuous Controller Results

The costs resulting from application of the Continuous Controller are briefly mentioned here, and the preliminary results from one Monte Carlo trial appear in Table 15. These values are computed for a spacecraft on the 2-year Lissajous path (depicted in Figure 1-4) in the vicinity of the interior libration point defined for the Sun-Earth+Moon system. The error models for each of the six states are listed vertically in the same order as the elements appear in the residual state vector; that is, $x, y, z, \dot{x}, \dot{y}, \dot{z}$. Tracking and injection errors are modeled at different levels and are thus listed separately. The errors

are represented in terms of mean and variance in the form $N(\mu,\sigma^2)$; where, of course, the mean is μ and the variance is σ^2.

The error levels used in Table 15 are clearly not those listed in Table 1 from the orbit determination error analysis investigation briefly described in Chapter 1.[24] This preliminary continuous control work was completed well before the error analysis was begun. Further work on the Continuous Controller is not anticipated at this time; the initial, partial results are only presented here for information and comparison purposes. The injection errors agree with those found in Rodriquez-Canabal[32], and the tracking errors correspond to those of Simó[40] for a libration point orbit.

Control input errors are computed as a percent deviation from the control command. The control errors are then input independently into each channel. The control inputs are continuous and at a constant magnitude in each control channel for either 30-day or 45-day steps in this study. The control inputs are then recalculated and input at the next computed level for the following 30 or 45 days. This method of computing control inputs is continued throughout the 2-year orbit. Position errors are expressed in kilometers and velocity errors in meters/second.

Table 15. Control Costs Associated with the Continuous Controller.

Bias and Random Error Sources			Two-Year Δv_T (meters/second)	
Injection	**Tracking**	**Control**		
N(100,0)	$N(0,1.5^2)$			
N(100,0)	$N(0,2.5^2)$			
N(100,0)	$N(0,15^2)$			
N(.05,0)	$N(0,.001^2)$	N(0,3%)	.1422	(30-Day Steps)
N(.05,0)	$N(0,.001^2)$			
N(.05,0)	$N(0,.003^2)$			
SAME AS ABOVE	SAME AS ABOVE	SAME AS ABOVE	.5362	(45-Day Steps)

The constant acceleration (in meters per second per second) used by the controller over a given period is easily converted to a Δv value for comparison with other controllers. The acceleration is constant over a given time step, and the equivalent delta-velocity can be computed by multiplying the constant acceleration by the duration of the time step in appropriate units.

The method used here provides results that are approximately equal to those presented in Breakwell et al.[33] In that study, an integral quadratic cost function is minimized to compute optimal state feedback control for a periodic halo-type orbit near the translunar libration point in the Earth-Moon system. The control accelerations of about 10^{-8} g's listed in Breakwell et al are slightly higher than the 8.0×10^{-9} g's that are approximately required for the method used here. It is interesting to note that the solar reflectivity uncertainty at the two standard deviation level is approximately 4.0×10^{-9} g's for this spacecraft in the libration point orbit.[42] A portion of the difference in required control levels may be attributed to the much larger value of μ in the Earth-Moon system versus the Sun-Earth+Moon three-body problem; the orbit used in Breakwell et al is also larger, in relation to the relative size of the respective three-body systems, than the nominal path used here. In addition, Breakwell et al assume that the only nonzero entries in the state error weighting matrix Q (that appears in the quadratic cost function) are those associated with position errors; velocity errors are unweighted.

The results listed in Table 15 clearly show that the Continuous Controller can maintain the spacecraft near the nominal Lissajous path for 2 years at a very low cost. However, operational requirements suggest that the On/Off Controller that incorporates the use of some minimum time between manuevers, minimal control input magnitudes, and a minimum deviation distance from the nominal path should be investigated. This On/Off Controller, while still using constant accelerative inputs over disjoint time periods, may more closely model possible thrust devices being developed now for use in the next decade.

b. On/Off Controller Results

The control costs associated with the On/Off Controller are larger than those found for cases that incorporate the delta-velocity controllers in this work. For comparison purposes, the accelerative inputs have been converted to equivalent delta-velocities and have been summed to reflect a 2-year total. The Δv_{min} value can also be converted in a similar way to find minimal accelerative force levels. For instance, a minimum Δv of .015 meters per second is equivalent to a minimum constant acceration of approximately 8.681×10^{-9} meters per second per second input for 20 days. A minimum Δv of .025 meters per second is equivalent to a minimum constant acceleration of approximately 1.4468×10^{-8} meters per second per second. The results from simulations in two cases that incorporate the On/Off Controller are summarized in Table 16. The notation is identical to that used in previous sections.

Table 16. Mean and Variance Levels Associated with On/Off Controller.

				Lissajous Orbit		Halo-Type Orbit	
#	Δt_{min} (days)	Δv_{min} (m/s)	d_{min} (km)	$\hat{\Delta v}_L$ (m/s)	s_L (m/s)	$\hat{\Delta v}_H$ (m/s)	s_H (m/s)
III-1	20	.015	100	.3255	.0428	.3661	.0785
III-2	40	.025	100	.7033	.2788	.6999	.2340

The equivalence of the population variances for Lissajous and halo-type orbits can now be tested. Again, Fisher's F test is used to test for equal population variances. The α level is set at .01, and the hypotheses and decision rule are given as:

Hypotheses:

$$H_0: \sigma_H^2 = \sigma_L^2.$$

$$H_1: \sigma_H^2 \neq \sigma_L^2.$$

Decision Rule:

If $F_{(29,29,.005)} \leq (s_H^2/s_L^2) \leq F_{(29,29,.995)}$, conclude H_0.

Otherwise, Conclude H_1.

The numerical results and conclusions of the hypothesis tests for equal variances are listed in Table 17. The notation is identical to that used in previous sections.

For both cases, the statistical hypothesis test for equality of population variances within each case for both Lissajous and halo-type orbits results in the conclusion that H_0 is, in fact, true. Notice that, if a slightly larger α risk were used, cases III-1 and III-2 would indicate that the two populations do not have equivalent variances. However, for these cases, we can, in fact, use the pooled variance equation and can then proceed with the tests for equal population means.

Table 17. Test Results for Equal Variances for the On/Off Controller

#	s_L (m/s)	s_H (m/s)	F_{low}	F^*	F_{up}	Conclusion
III-1	.0488	.0785	.3704	2.5876	2.700	H_0
III-2	.2788	.2340	.3704	.7044	2.700	H_0

The next step in this analysis is to test for equivalent Δv_T population means. The test again uses the student's t distribution, and an α value of .01 is used. The hypotheses and the decision rule are given by:

Hypotheses:

$H_0: \mu_L = \mu_H$.

$H_1: \mu_L \neq \mu_H$.

Decision Rule:

If $-t \leq t^* \leq t$, conclude H_0.

Otherwise, conclude H_1.

The α risk of .01 is again equally divided in both tails of the t distribution. The degrees of freedom are, for this hypothesis test, equal to $(n_L-1) + (n_H-1)$ and the t statistic is $\pm t_{(.995,58)} = \pm 2.66$. The numerical results and the conclusions of these tests are listed in Table 18. The notation used here is identical to that used in previous sections.

Table 18. Results of Tests for Equal Means for the On/Off Controller.

#	$\hat{\Delta v}_L$ (m/s)	$\hat{\Delta v}_H$ (m/s)	-t	t^*	t	Conclusion
III-1	.3255	.3661	-2.66	-2.49	2.66	H_0
III-2	.7033	.6999	-2.66	.1011	2.66	H_0

For both control options III-1 and III-2, the conclusion is that the population means are equal with 99% confidence. Clearly, with an α risk slightly greater than 1%, control option III-1 would lead to the conclusion that the two populations have unequal means.

It might be interesting to end this section with a short comparison of costs produced using the On/Off Controller with those resulting from simulations with the Delta-Velocity Controller I. This comparison should be completed with the note that the two types of

controllers (delta-velocity and on/off) are, in fact, fundamentally different. Some cases are compared in Table 19 by using confidence intervals for the mean. The significant overlap of the confidence intervals for cases I-1 and III-1 and for cases I-3 and III-2 illustrate the similarity in control costs.

Table 19. Comparison of Costs Resulting from Use of Controller I and the On/Off Controller.

#	Lissajous Orbit (m/s)		Halo Orbit (m/s)	
	Lower Limit	Upper Limit	Lower Limit	Upper Limit
I-1	.2946	.3607	.3073	.3717
III-1	.3063	.3477	.3309	.4013
I-3	.7187	1.1020	.4860	1.3030
III-2	.5780	.8286	.5947	.8051

In comparing the station-keeping costs, the agreement observed between results from use of these two differing methods is interesting. However, the On/Off Controller produces costs that are somewhat higher in general than Controlier II, and its performance when the minimum manuever separation time is extended to 60 or 80 days is disappointing. Future work in this area is anticipated and may prove valuable. The last section of this chapter contains a survey of the station-keeping costs found in several other libration point station-keeping studies. It also includes some of the results from this work.

4. Survey of Libration Point Orbit Station-Keeping Costs

For completeness, it is important to consider how libration point orbit station-keeping costs can be compared. Certainly the cost of maintaining the spacecraft in orbit for 2 years could be a common comparison value. However, the real difficulty here is also closely related to the focus of the error analysis investigations in Chapter 1

of this work. A general lack of consistency in input error levels for both orbit determination error analysis and station-keeping studies for libration point orbits has been noted. Some of this inconsistency can be attributed to differing equipment and missions. Some cannot. Two papers[62,63] concerning the same set of studies, for instance, disagreed on the variances associated with the tracking errors that were used in the station-keeping simulations.

Most studies do not address the fact that the control costs from a sequence of Monte Carlo station-keeping simulations are random variables. Each random trial will provide a different result. It is assumed here that the results published in most studies are actually the sample means of the station-keeping costs. One study[9,27] has provided substantial statistical details in an excellent station-keeping study that could allow the construction of confidence intervals for the mean costs in that work. Such completeness of data presentation is in general lacking in other station-keeping studies, and any assumptions that must be made about the data will be stated clearly in this work.

The results of several station-keeping studies are presented in Table 20. The methods are listed in order of publication date; each reference is listed by its bibliography number and below it is the date of publication. Actual flight data is given for ISEE-3. The input error levels, if available, are included as standard deviations in the order consistent with the residual state vector $(x,y,z;\dot{x},\dot{y},\dot{z})$, with position state errors given in kilometers and velocity state errors given in milimeters per second. The standard deviations for solar reflectivity uncertainty are listed as a percent of the nominal value. The control uncertainty is a one standard deviation error listed as a percent of the commanded control, usually input independently in each of the three possible channels.

Table 20. Survey of Station-Keeping Costs for Two-Year Halo Orbits.

SUN-EARTH L1 HALO ORBIT STATION-KEEPING ERRORS AND CONTROL COSTS					
Source	Tracking Errors	Solar Reflectivity Uncertainty	Control Errors	2-Year Cost (m/s)	Remarks
[65] (1977)	3,30,30 km; 15,15,30 mm/s	N/A	10%	15.24 26.60	Δt_{min}=30 da Δt_{min}=60 da
ISEE-3 [79,80] (1982)	N/A	N/A	N/A	15.0	Actual Flight Data
[60] (1984)	2.7,3.9,3.4 km; 2.4,3.5,1.3 mm/s	10%	N/A	.08	4 cm/s/yr
[62] (1986)	1.5,2.5,15 km; 1,1,3 mm/s	2.5%	2.5%	0.4	20 cm/s/yr
[63] (1987)	1.7,2.2,5.5 km; 1.4,1.4,2.4 mm/s	5.0%	2.5%	0.4	.7-.8 m/s/ 4 yrs
[64] (1989)	$\lvert(x,y,z)^T\rvert \leq$ 20 km; $\lvert(\dot{x},\dot{y},\dot{z})^T\rvert \leq$ 15 mm/s	5.0%	5.0%	1.3	4 m/s/ 6 yrs
[12,91] (1990)	1.5,2.5,15 km; 1,1,3 mm/s	N/A	2.5%	0.8	Δt_{min}=60 da (one of many cases)
This Work	1.46,2.64,4.81 km; 1.4,1.85,2.49 mm/s	13%	10.0%	0.81 (.76-.87) 1.1 (.92-1.23)	Δt_{min}=60 da Δt_{min}=80 da

The station-keeping expenses are listed as 2-year costs. When a study has printed the station-keeping cost for other than a 2-year value, this cost is computed and the actual cost from the study is included in the "remarks" column. For the control costs computed in this work, both the mean value and then the 99% confidence interval limits (in parentheses) are listed. If the level of errors used in a given study is not available, an "N/A" is indicated in the appropriate column. The error levels used to model orbit injection errors are not listed in Table 20. In most of these studies, injection errors were modeled at the same level as tracking errors. In some cases, the injection errors were modeled at slightly higher levels; however, at these higher levels, the injection errors generally contribute only about 15% or less to the station-keeping costs.

Clearly, there appears to be a wide disparity in the station-keeping costs predicted for a spacecraft in a halo or halo-type orbit near L_1 in the Sun-Earth system. Some of these differences can be explained by the disagreement in error levels; some can be attributed to the variety of station-keeping algorithms. Also, these studies do not consider the same nominal orbit. A control cost such as the 0.8 meters per second for 2 years found in Howell and Pernicka[9,27] seems to be quite reasonable. This cost is certainly a great improvement over the 7.62 to 13.3 meters per second per year predicted for ISEE-3 and the actual mission results showing approximately 30 meters per second expended for less than 4 years on station. Further work developing station-keeping routines that can tolerate longer minimum times between manuevers (Δt_{min}), increased error levels, and the inclusion of a larger d_{min} may be beneficial. Investigations concerning the "optimal" selection of weighting matrix entries may enable existing methods, such as those described in this work, to provide much improved results. Furthermore, the selection of target times and control input times for these methods may also be fruitful areas for future research.

LIST OF REFERENCES

1. S.C. Gordon, "Some Results of Adding Solar Radiation Pressure Forces to the Restricted Three-Body Problem," USAFA TR 91-10, September 7, 1991.

2. R.W. Farquhar, "The Control and Use of Libration-Point Satellites," Ph.D. Dissertation, Department of Aeronautics and Astronautics, Stanford University, Stanford, California, July 1968.

3. R.W. Farquhar, "A Halo-Orbit Lunar Station," *Astronautics and Aeronautics*, June 1972, pages 59-63.

4. J.R. Wertz, Editor, *Spacecraft Attitude Determination and Control*, D. Reidel Publishing Co, Boston, 1978.

5. S. Wolf, *Guide to Electronic Measurements and Laboratory Practice*, Prentice Hall, Englewood Cliffs, New Jersey, 1973.

6. R.W. Farquhar and A.A. Kamel, "Quasi-Periodic Orbits About the Translunar Libration Point," *Celestial Mechanics*, Volume 7, 1973, pages 458- 473.

7. D.L. Richardson and N.D. Cary, "A Uniformly Valid Solution for Motion About the Interior Libration Point of the Perturbed Elliptic-Restricted Problem," AAS/AIAA Astrodynamics Specialists Conference, Nassau, Bahamas, July 28-29, 1975, AAS Paper 75-021.

8. D.L. Richardson, "Halo Orbit Formulation for the ISEE-3 Mission," *Journal of Guidance and Control*, Volume 3, Number 6, November-December 1980, pages 543-548.

9. H.J. Pernicka, "The Numerical Determination of Nominal Libration Point Trajectories and Development of a Station-Keeping Strategy," PhD Dissertation, School of Aeronautics and Astronautics, Purdue University, West Lafayette, Indiana, May 1990.

10. H.J. Pernicka, "The Numerical Determination of Lissajous Orbits in the Circular Restricted Three-Body Problem," M.S. Thesis, School of Aeronautics and Astronautics, Purdue University, West Lafayette, Indiana, December 1986.

11. K.C. Howell and H.J. Pernicka, "Numerical Determination of Lissajous Trajectories in the Restricted Three-Body Problem," *Celestial Mechanics*, Volume 41, 1988, pages 107-124.

12. K.C. Howell, Principal Investigator, "Trajectory Design for Libration Point Trajectories and for Double Lunar Swingby Trajectories," Final Report Prepared for Computer Sciences Corporation, December 1987.

13. K.C. Howell, Principal Investigator, "Design of Libration Point Trajectories and Consecutive Lunar Encounter Trajectories," Final Report Prepared for Computer Sciences Corporation, September 1988.

14. H.J. Pernicka, "The Numerical Determination of Libration Point Trajectories, Including Development of Station-Keeping Strategies," Proposal for Dissertation, School of Aeronautics and Astronautics, Purdue University, West Lafayette, Indiana, December 1988.

15. S.C. Gordon, Representing the Nominal Path for an Interior Libration Point Orbit in the Sun-Earth+Moon Elliptic Restricted Three-Body Problem," USAFA TR 91-11, September 7, 1991.

16. J.L. Bell, Private Communication, School of Aeronautics and Astronautics, Purdue University, West Lafayette, Indiana, August, 1990.

17. The MathWorks, *386-Matlab*, 21 Eliot Street, South Natick, Ma, 1989.

18. V. Szebehely, *Theory of Orbits: The Restricted Problem of Three Bodies*, Academic Press, New York, 1967.

19. A.E. Roy, *Orbital Motion*, Second Edition, Adam Hilger Ltd, Bristol, England, 1982.

20. E.A. Grebenikov, "On the Stability of the Lagrangian Triangle Solutions of the Restricted Elliptic Three-Body Problem," *Soviet Astronomy*, Volume 8, Number 3, November-December 1964, pages 567-578.

21. J.M.A. Danby, "Stability of the Triangular Points in Elliptic Restricted Problem of Three Bodies," *The Astronomical Journal*, Volume 69, Number 2, March 1964, pages 165-172.

22. A. Bennett, "Characteristic Exponents of the Five Equilibrium Solutions in the Elliptically Restricted Problem," *Icarus*, Volume 4, 1965, pages 177-190.

23. D.L. Richardson, "Analytic Construction of Periodic Orbits About the Collinear Points," *Celestial Mechanics*, Volume 22, 1980, pages 241-253.

24. S.C. Gordon, "Orbit Determination Error Analysis for an Interior Libration Point Orbit in the Sun-Earth+Moon Elliptic Restricted Three-Body Problem," USAFA TR 91-12, September 7, 1991.

25. N.P. Dwivedi, "Manuever Strategies for Multi-Planet Missions," AIAA Astrodynamics Conference, Palto Alto, California, Septemper 11-12, 1972, AIAA Paper 72-914.

26. N.P. Dwivedi, "Deterministic Optimal Manuever Strategy for Multi-Target Missions," *Journal of Optimization Theory and Applications,* Volume 17, Number 1/2, 1975, pages 133-153.

27. K.C. Howell and H.J. Pernicka, "A Station-Keeping Method for Libration Point Trajectories," Proceedings of the AIAA/AAS Astrodynamics Conference, Portland, Oregon, ugust 1990, pages 713-723.

28. R.E. Skelton, *Dynamic System Control*, John Wiley and Sons, New York, 1988.

29. R.E. Skelton, A.M. King, "Steady State LQG Theory for Time Invariant Systems," School of Aeronautics and Astronautics, Purdue University, West Lafayette, Indiana, 1989.

30. A.E. Bryson Jr., Yu-Chi Ho, *Applied Optimal Control*, Blaisdell Publishing Co, Waltham, Massachusetts, 1969.

31. H. Kwakernaak, R. Sivan, *Linear Optimal Control Systems*, Wiley-Interscience, New York, 1972

32. J. Rodriquez-Canabal, M. Hechler, "Orbital Aspects of the SOHO Mission Design," AAS Preprint 89-171-01, 1989.

33. J.V. Breakwell, A.A. Kamel, M.J. Ratner, "Station-Keeping for a Translunar Communications Station," *Celestial Mechanics,* Volume 10, pages 357-373, 1974.

34. W.L. Brogan, *Modern Control Theory*, Prentice-Hall, Inc., Newark, New Jersey, 1985.

35. R.E. Kalman, "Contributions to the Theory of Optimal Control," *Bol. de Soc Math Mexicana,* 1960, pages 102-119.

36. R.H. Battin, *An Introduction to the Mathematics and Methods of Astrodynamics*, AIAA Education Series, New York, 1987.

37. W.T. Reid, *Riccati Differential Equations*, Mathematics in Science and Engineering, Volume 86, Academic Press, New York, 1972.

38. A. Gelb, Editor, *Applied Optimal Estimation*, The M.I.T. Press, Cambridge, Massachusetts, 1974.

39. J. Neter, W. Wasserman, G.A. Whitmore, *Applied Statistics,* Allyn and Bacon, Boston, 1988.

40. C. Simó, G. Gómez, J. Llibre, R. Martinez, "Station Keeping of a Quasiperiodic Halo Orbit Using Invariant Manifolds," Proceedings of the Second International Symposium on Spacecraft Flight Dynamics, Darmstadt, Federal Republic of Germany, 20-23 October 1986.

41. G. Simó, G. Gómez, J. Llibre, R. Martinez, J. Rodriquez, "On the Optimal Station Keeping Control of Halo Orbits," *Acta Astronautica*, Volume 15, Number 6/7, 1987, pages 391-397.

42. J.M. Longuski, R.E. Todd, "A Survey of Nongravitational Forces and Space Enviornmental Torques with Applications to the Galileo Spacecraft," School of Aeronautics and Astronautics, Purdue University, West Lafayette, Indiana, 1990.